CHAPTER 6

Effect of Channel Designs and Its Optimization for Enhanced Thermo-hydraulic Performance of Solar Air Heater

Rising future energy demands can be met with solar-based devices such as solar air heaters (SAH) only if the efficiency of these devices is enhanced with suitable design changes. Flow channel design of a SAH is an essential aspect for enhancing its thermo-hydraulic performance for a wide range of Reynolds numbers. In this chapter, a systematic approach has been adopted to investigate various non-rectangular channel designs numerically, and results are compared with the conventional rectangular design. The energy input to all designs is kept constant. The channel design that gives the best performance was further investigated by incorporating a sinusoidal wavy absorber having variable wavy roughness parameters. The flow and heat transfer characteristics have been evaluated in terms of friction factor (f) and Nusselt number per unit friction factor (Nu/f), temperature factor $\left(\frac{T_0-T_i}{I}\right)$, thermal effectiveness (ε), Nusselt number (Nu). The results show that the SAH duct having a semi-ellipse cross-section offers the best thermo-hydraulic performance and has maximum augmentation in temperature factor of about 10% compared to conventional SAH. Moreover, semi-ellipse SAH with sinusoidal wavy absorber has a maximum value of $f/f_s$and Nu/Nu_s at $A/D_h = 0.12$ and $\lambda/D_h = 0.8$ for the range of Reynolds numbers used. Here,A is the amplitude and λ is the wavelength of the absorber plate. New empirical relationships for Nu and f are established as a function of flow and geometric parameters that agree well with numerical results.

6.1 Introduction

With rising population, demand for energy use is also increasing exponentially. Since the human race has been utilizing energy from conventional fuels such as crude oil, coal, etc., for a long duration of time, therefore, those recourses are depleting dynamically[115, 141]. Alternative energy sources such as solar energy is complementing conventional sources of energy, nonetheless, low efficiency of these devices comes in the way of wide applicability of these solar-based devices. One of the versatile solar based devices is SAH, which is used for crop drying [41], space heating[88, 143], laundry drying [55] etc. Previous researchers have made various attempts to increase the efficiency of the SAH. Since design plays a significant role in enhancing the thermal efficiency of the SAH, most of the previous investigations have focused on changing the designs (see Table 6.1). In general, SAH consist of a rectangular cross-sectional shape flow channel with its top surface as absorber plate (i.e. conducting material) and the insulated bottom through which the air flows. The solar radiation that falls on the absorber surface heats the plate, and consequently, the airflow gets heated during interaction with the hot absorber surface. The availability of high intense solar radiation is approximately 4 to 6 hours/day; in this short period, the SAH device must be thermally more effective to utilize substantial portion of available solar energy.

There have been many ideas proposed in the literature to augment the thermal performance of the SAH devices. These ideas were observed generally in terms of change in the design of cross-section shape [56, 100, 128], absorber surface[61, 87, 90, 111, 124, 130, 138] and flow passage [2, 74, 104] of SAHs. Various forms of extended bodies such as fin, rib and groove have been implemented on the smooth plate of the absorber to promote turbulence in the airflow. The thermal performance augmentation of the SAH device is generally observed with increased pressure drop. The power needed to pump the fluid in the flow channel of SAH increases with increase in hydraulic (frictional) losses, due to hindrance offered under the existence of extended surfaces (ribs, fins, etc.) in the flow channel.

Table 6.1: The list of previous studies to augment thermal performance using different cross-sectional shape and corrugated shape of absorber surface in the flow channel.

Investigator	Cross-sectional shape	Absorber shape	Finding

Table 6.1: The list of previous studies to augment thermal performance using different cross-sectional shape and corrugated shape of absorber surface in the flow channel.

Karim and Hawlader [68]	Rectangular		The flat plate SAH is 5 – 11% and 10 – 15% less efficient in double and single-pass mode than V-corrugated SAH.
Singh and Negi [131]	Rectangular	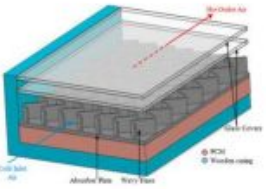	PCM integrated with corrugated finned SAH has 64% more thermal efficiency than flat-plate SAH with PCM.
Lin et al. [86]	Rectangular	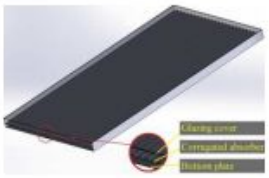	Surface absorptance and opening angle were the most crucial design variable on which thermal efficiency of corrugated SAHs depends.
Pehlivan et al. [106]	Rectangular	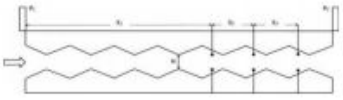	Corrugated channel SAH should be used in high heat flux applications or more efficient heat exchange devices. For Re = 1500 - 8000and Nu/Nu_s=1.50 - 4.30.
Singh[128]	Semicircular and triangular	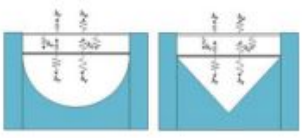	Model-II with recycling has 3 – 17% lesser thermal efficiency than Model-I

Table 6.1: The list of previous studies to augment thermal performance using different cross-sectional shape and corrugated shape of absorber surface in the flow channel.

Gao et al.[34]	Rectangular	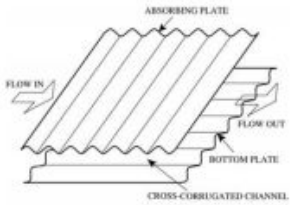	SAH with wavelike shape of absorber perpendicular to flow direction and that bottom plate along the flow direction has more thermal performance as compare to SAH with just opposite corrugation of absorber and bottom plate along the flow direction.
Kareem et al.[66]	Circular	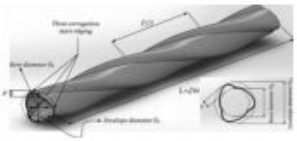	Smooth spiral corrugation has 2.4-3.7 times more heat transfer than smooth tube. For Re = 100 -1300 and Nu/Nu_s=2.4 - 3.7
Kumar et al.[82]	Triangular	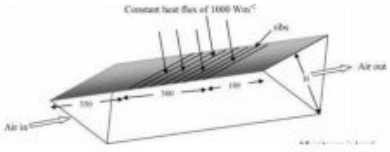	Triangular cross-sectional duct SAH with a chamfered ribbed absorber plate has Nusselt number 3.52 times more than without rib triangular cross-sectional duct SAH. For Re = 4000 - 18000 and Nu/Nu_s=1.74 - 2.48.

Table 6.1: The list of previous studies to augment thermal performance using different cross-sectional shape and corrugated shape of absorber surface in the flow channel.

Nidhul et al.[99]	Triangular	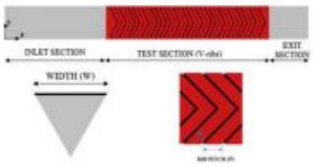	For a higher mass flow rate, the ribbed triangular duct has better performance over the exact configuration of the ribbed rectangular duct. For Re = 5000 - 20000 and Nu/Nu_s=1.45 - 2.41.
Kumar and verma [84]	Rectangular	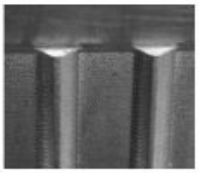	SAH with sinusoidal rib on absorber surface has 20.06% and 33.31% higher thermal-hydraulic performance than the same SAH with triangular and square ribs on the absorber surface. For Re = 4000 -15000 and Nu/Nu_s=2.25 - 2.48.
Manjunath et al.[91]	Rectangular	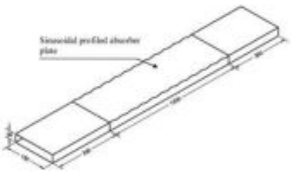	Sinewave corrugation SAH has higher and lowers effective efficiency than conventional SAH for lower and higher air mass flow rates. For Re = 4000 - 24000 and Nu/Nu_s=1.39 - 2.78.
Present study	Semi-ellipse		The value of Nu/f is maximum at A/D_h=0.4 and λ/D_h=0.8. For Re =11000 - 19000 and Nu/Nu_s=1.42 - 3.20.

It can be observed from Table 6.1 that plenty of research has been performed on the rectangular cross-sectional shape of SAH (conventional SAH) with artificial ribs, fin and various configuration of corrugation. For a same energy input, how a non-rectangular channel de-

Table 6.2: Range of geometrical and flow parameters.

S.No	Parameters	Parametric values
1	Relative roughness wavelength (λ/D_h)	0.8, 1.2 *and* 1.6
2	Relative roughness amplitude (A/D_h)	0.04, 0.08 *and* 0.12
3	Reynolds number (Re)	11000 – 19000
4	Heat flux (q)	500 W/m^2

sign affects the thermal performance of a SAH is still not yet explored in detail.The use of non-rectangular channels such as trapezoidal, isosceles triangular and semi-ellipse designs are novel design ideas. When the energy input to a given SAH design remains the same, which type of channels design would show better thermal performance is still an open question that should be investigated. This paper explores the stated question. The aim of this paper is multifold: First, to develop a validated numerical model to study the various channel designs of a SAH; second, to examine the thermal performance of various channel designs for a large range of governing parameters; third, to further optimize the best channel configuration that significantly enhances the flow mixing and thermal performances of the SAH; and fourth, to develop correlations for Nu and f as function of flow and geometric parameters to facilitate the prediction of thermal and hydraulic performances of the optimum design. The systematic investigations and results illustrated in this article would assist investigators in developing efficient designs of SAH.

6.2 Description of problem

The 3-D geometry of forced convection SAH has been studied for different cross-sections with smooth absorber (Fig.6.1a). After studying their performance, the best design was further optimized and avenues for additional increase in efficiency was explored as illustrated in Fig.6.1b The area of the absorber surface was kept constant for all the designs to keep the same energy input to the system.

The computational flow domain comprises the top surface (absorber plate) and bottom surface, inlet and outlet section. Constant heat flux was imposed on the absorber plate. The working fluid passes through the inlet section at a particular Reynolds number, heat from the hot absorber plate and exits from the outlet section. In the case of the best cross-section SAH with a wavy absorber, the corrugation parameters are defined by wavelength (λ) and amplitude (A). Wavy parameters are presented in the form of dimensionless numbers as relative roughness wavelength (λ/D_h) and relative roughness amplitude (A/D_h). Each SAH design has been investigated for Re in the range of 11000 – 19000. The flow and geometrical parameters are listed in Table 6.2.

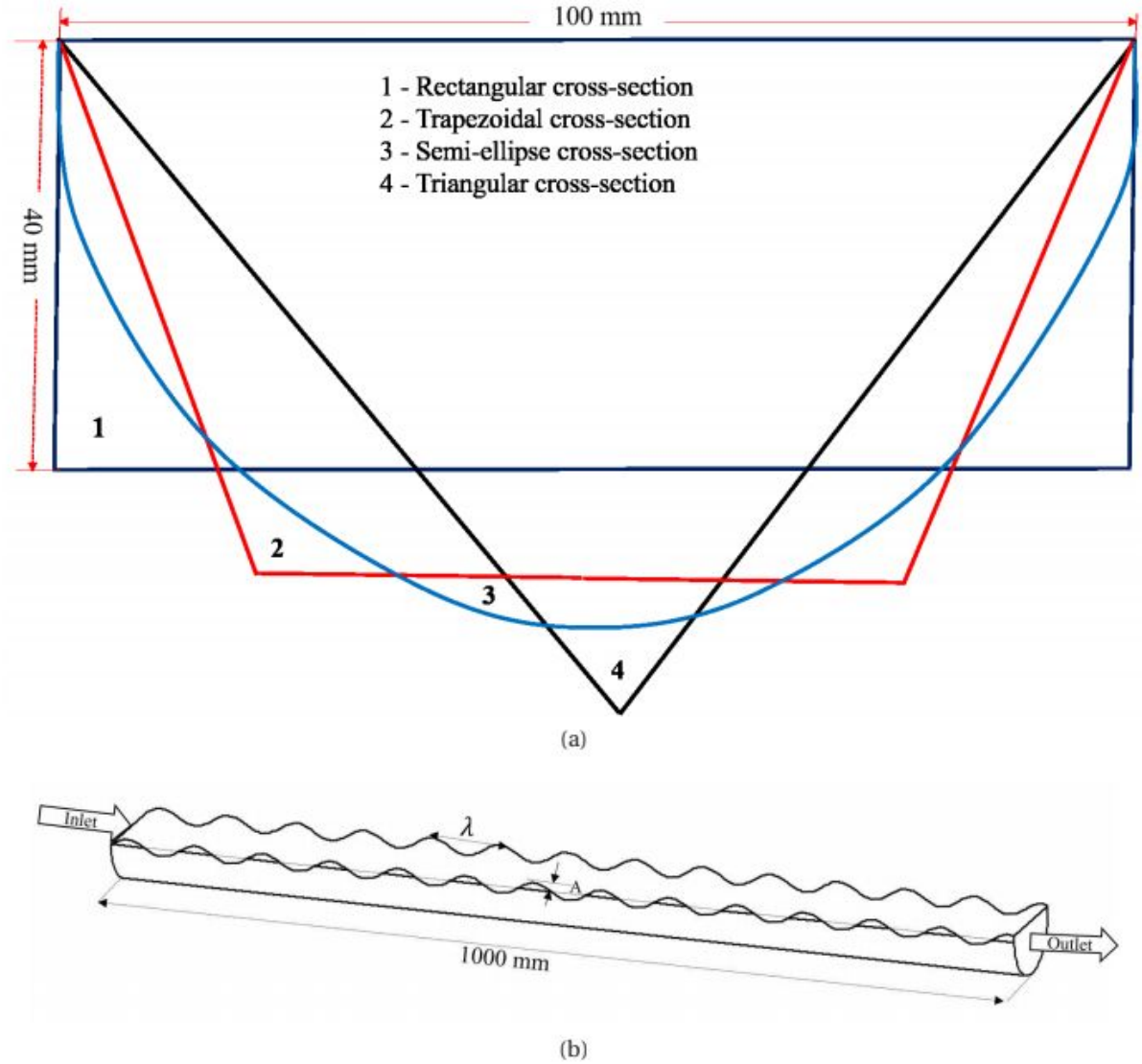

Figure 6.1: Schematic diagram of (a) Cross-sectional view (b) 3D view with wavy absorber plate.

6.3 The numerical model

6.3.1 *Grid generation and independence test*

Figure 6.2 shows the mesh generated for the rectangular cross-section SAH. Very fine mesh was created across the domain, including on the solid surfaces, to capture the thermal and velocity gradient effect. The same procedure of mesh generation was adopted for other designs. In computational fluid dynamics (CFD) modelling, the number of grids in the domain effects the solution accuracy and computational time, especially when the model is 3D. Hence, it is necessary to use optimum grids and report the results that are not dependent on grid sizes. A grid independence test was conducted using a different number of grid sizes. Five different number of grid elements was adopted with the same combination of boundary condition and model. As

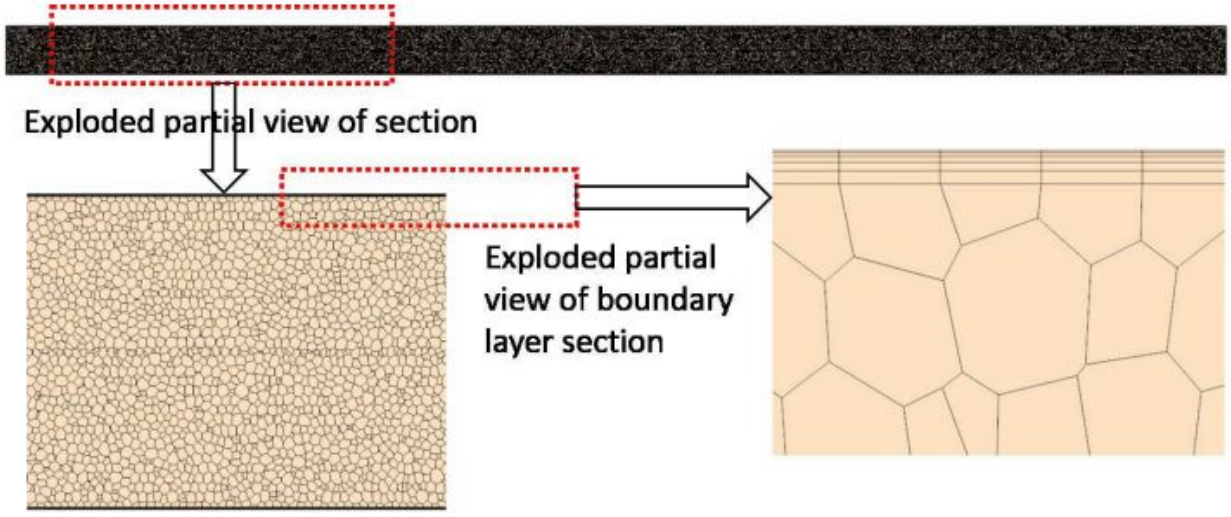

Figure 6.2: View of mesh generated for the rectangular cross-section SAH.

grid element changes from $2.07 * 10^5$ to $2.96 * 10^5$, $2.96 * 10^5$ to $4.34 * 10^5$, $4.34 * 10^5$ to$5.50 * 10^5$ and $5.50 * 10^5$ to $7.32 * 10^4$, the percentage variation in Nusselt number and air outlet temperature observed 1.88%, 1.04%, 1.0% and 0.89% and 0.3%, 0.12%, 0.11% and 0.005% respectively. Based on the above outcomes, the optimum number of elements has been chosen as $5.5 * 10^5$ for the entire study.

6.3.2 *Boundary conditions*

A fixed value of heat flux ($I = 500 W/m^2$) was applied to the top surface of SAH[4]. The velocity inlet condition was set at inlet section (i.e. at a specific value of Re). The outlet section of the SAH was assigned as pressure outlet condition (i.e. atmospheric condition). All cases were studied in the range of Re values of $11000 - 19000$. The air is modelled as an ideal gas. Physical properties air was assumed constant at 27^oC temperature. The values of the properties used as thermal conductivity(k) : $0.026 W/mK$, dynamic viscosity (μ) : $1.855 * 10^5 Ns/m^2$, and specific heat (Cp) : $1003.62 J/kgK$.

6.3.3 *Governing equations and turbulence model*

SIMPLE (semi-implicit method for pressure-linked equations) algorithm with finite volume method was used to solve the following governing equations for mass, momentum and energy. Realizable $k-\varepsilon$ turbulence model was employed to resolve the turbulent stresses in terms of the mean flow velocity gradient. Readers can refer to the previous paper [74, 123] by the same group on selecting various turbulence models and their accuracy in predicting thermal behavior in SAH application. Radiation losses from the glass are taken care by applying suitable boundary conditions.

Continuity equation

$$\nabla.(\rho V) = 0 \tag{6.1}$$

Momentum equations

$$\nabla.(\rho uV) = -\frac{\partial p}{\partial x} + \mu\nabla(\nabla.u) - \nabla\left(\overline{u'V'}\right) \tag{6.2}$$

$$\nabla.(\rho vV) = -\frac{\partial p}{\partial y} + \mu\nabla(\nabla.v) - \nabla\left(\overline{v'V'}\right) + \rho g_y \tag{6.3}$$

$$\nabla.(\rho wV) = --\frac{\partial p}{\partial z} + \mu\nabla(\nabla.w) - \nabla\left(\overline{w'V'}\right) \tag{6.4}$$

Energy equation

$$\nabla.(\rho VT) = \nabla.\nabla((\Gamma + \Gamma_t)T) \tag{6.5}$$

Where,

$$\Gamma_t = \frac{\mu_t}{Pr_t} and\, \Gamma = \frac{\mu}{Pr} \tag{6.6}$$

The turbulent dissipation rate (ε) and turbulent kinetic energy (k) are determined by using the Realizable $k-\varepsilon$ turbulence model and given as

$$\nabla.(\rho KV) = \nabla.\nabla(K(\mu + \frac{\mu_t}{\sigma_K})) + G_K + G_b \tag{6.7}$$

And

$$\nabla.(\rho\varepsilon V) = \nabla.\nabla\left(\varepsilon(\mu + \frac{\mu_t}{\sigma_\varepsilon})\right) - \rho C_{2\varepsilon}\frac{\varepsilon^2}{(K + \sqrt{\nu\varepsilon})} - C_{1\varepsilon}\frac{\varepsilon}{K}C_{3\varepsilon}G_b \tag{6.8}$$

The turbulent dynamic viscosity is determined as:

$$\mu_t = \rho C_\mu \frac{K^2}{\varepsilon} \tag{6.9}$$

where $C_{1\varepsilon}$, $C_{2\varepsilon}$, $C_{3\varepsilon}$ and C_μ are turbulence model constants and given as $C_{1\varepsilon}$ =1.44, , $C_{2\varepsilon}$ =1.92, , $C_{3\varepsilon}$ = - 0.33, C_μ = 0.09, σ_k= 1.0, σ_ε = 1.3

Reynolds number

$$Re = \frac{Inertia force}{Viscous force} = \frac{(\rho U D_h)}{\mu} \tag{6.10}$$

6.3.4 *Performance parameters*

To analyze the thermo-hydraulic performance of each SAHs, average absorber plate temperature (T_{mp}), mass flow average outlet temperature of air (T_0) and pressure loss through the SAHs

duct are determined. With the help of these parameters, five performance parameters such as temperature factor$\left(\frac{T_0-T_i}{I}\right)$, thermal effectiveness (ε), Nusselt number (Nu), Nusselt number per unit friction factor (Nu/f) and friction factor (f) are calculated and performance of various designs are compared. Above parameters are defined below.

Temperature factor is the ratio of change in temperature of air at outlet and inlet of the duct per unit solar radiation fall on the absorber surface, i.e., [73]

$$TF = \left(\frac{T_0 - T_i}{I}\right) \tag{6.11}$$

Thermal effectiveness is the measure of thermal characteristic associated with SAH device. It is defined as [122]

$$\varepsilon = \left(\frac{T_0 - T_i}{T_{mp} - T_i}\right) \tag{6.12}$$

The useful energy gain by air in SAH is calculated as

$$Q = \dot{m}C(T_0 - T_i) \tag{6.13}$$

As fluid flow over the absorber surface the velocity boundary layer changes in the flow direction. Consequently, local heat transfer coefficient varies along the absorber surface and is given as

$$h_x = \frac{q_s^{''}}{\left(T_{surface,x} - T_{bulk,x}\right)} \tag{6.14}$$

The total convection heat transfer rate 'Q' is the integral of the surface heat flux $\left(q_s^{''}\right)$ over the whole absorber surface area (Aeff):

$$Q = \int_0^{A_{eff}} q_s^{''} dA_s \tag{6.15}$$

Thus the average heat transfer coefficient can be calculated as[132]

$$h = \left[\frac{Q}{A_{eff}(T_{mp} - T_m)}\right] \tag{6.16}$$

Which is also related to h_x by

$$h = \frac{1}{A_{eff}} \int_0^{A_{eff}} h_x dA_s \tag{6.17}$$

where T_m is the bulk mean temperature of fluid which is the average of outlet air temperature (T_0) and inlet air temperature (T_i).

Local Nusselt number Nu_x

$$Nu_x = \frac{h_x D_h}{k} \tag{6.18}$$

Average Nusselt number is represented as

$$Nu = \frac{hD_h}{k} \tag{6.19}$$

where D_h is characteristic diameter of SAH, which is defined as [93]

$$D_h = \frac{4A_{cross}}{P} \tag{6.20}$$

Darcy friction factor is determined by using Darcy-Weisbach equation as [93]

$$f = \frac{2\Delta P D_h}{\rho L U^2} \tag{6.21}$$

At inlet boundary condition, turbulent intensity is determined as [96]

$$TI = 0.16\, Re^{\left(-\frac{1}{8}\right)} \tag{6.22}$$

Results from numerical model are also used to compared the values of Nusselt number and friction factor for the smooth duct of SAH using Dittus–Boelter equation and Blasius equations, respectively as:

Dittus-Boelter equation[145]

$$Nu = 0.023 Re^{0.8} pr^{0.4} \tag{6.23}$$

Blasius equations[145]

$$f = 0.0791 Re^{-0.25} \tag{6.24}$$

6.3.5 *Validation of computational model*

The present numerical results are compared with an experimental[35] and theoretical correlation (Dittus-Boelter and Blasius correlations) results to ensure the precision of numerical model. For this same geometrical and operating boundary conditions ($q = 1000\, W/m^2$) were used as mentioned in the experimental study of Gawande et al.[35]. The present numerical results have an average absolute standard deviation of about 4.24% and 2.98% for Nu and f, respectively, from experimental results (Fig. 6.3 and Fig.6.4). When it is compared with the theoretical study, the average absolute deviation is 6.73% and 3.78% for Nu and f, respectively. Hence, present numerical work can be applied to further studies.

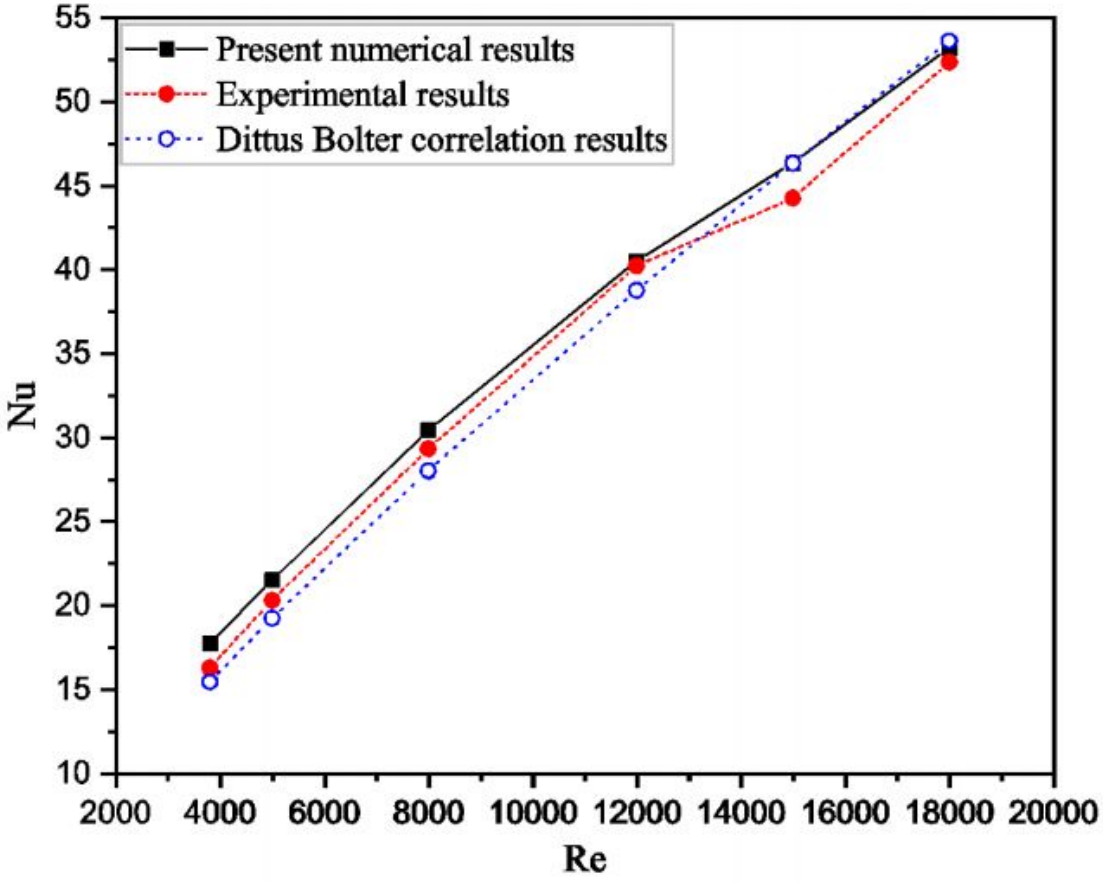

Figure 6.3: Comparison among numerical, experimental and predicted results of Nusselt number for smooth duct.

6.4 Results and Discussion

6.4.1 *Results of different cross-sectional SAHs*

Figure 6.5 represents the variation of temperature factor$\left(\frac{T_0-T_i}{I}\right)$, with Reynold number($Re$). With increase in Re, the residence time of fluid inside the duct also declines. Therefore, temperature factor decrease with increase of Re. The maximum percentage rise of $9-10\%$ in temperature factor has been seen for SAH duct having semi-ellipse cross-section compared to the rectangular cross-section. While the next maximum is $4-5\%$ increase for the trapezoidal cross-section. The triangular cross-section is inferior to conventional rectangular SAH duct. The order of hydraulic diameters has been found to be in descending order as: semi-ellipse > trapezoidal >rectangular > triangular. Consequently, the inlet velocity of fluid is lower in semi-ellipse cross-section as compare to other cross-sectional SAHs. Therefore, working fluid has a larger residence time in semi-ellipse cross-section than other cross-sections of SAHs.

Figure 6.6 shows the distribution of local heat transfer coefficient (h_x) along the length of absorber (Y/L= 0, X/L = 0.05 and Z/L) of SAH with different cross-section for two case of Reynolds

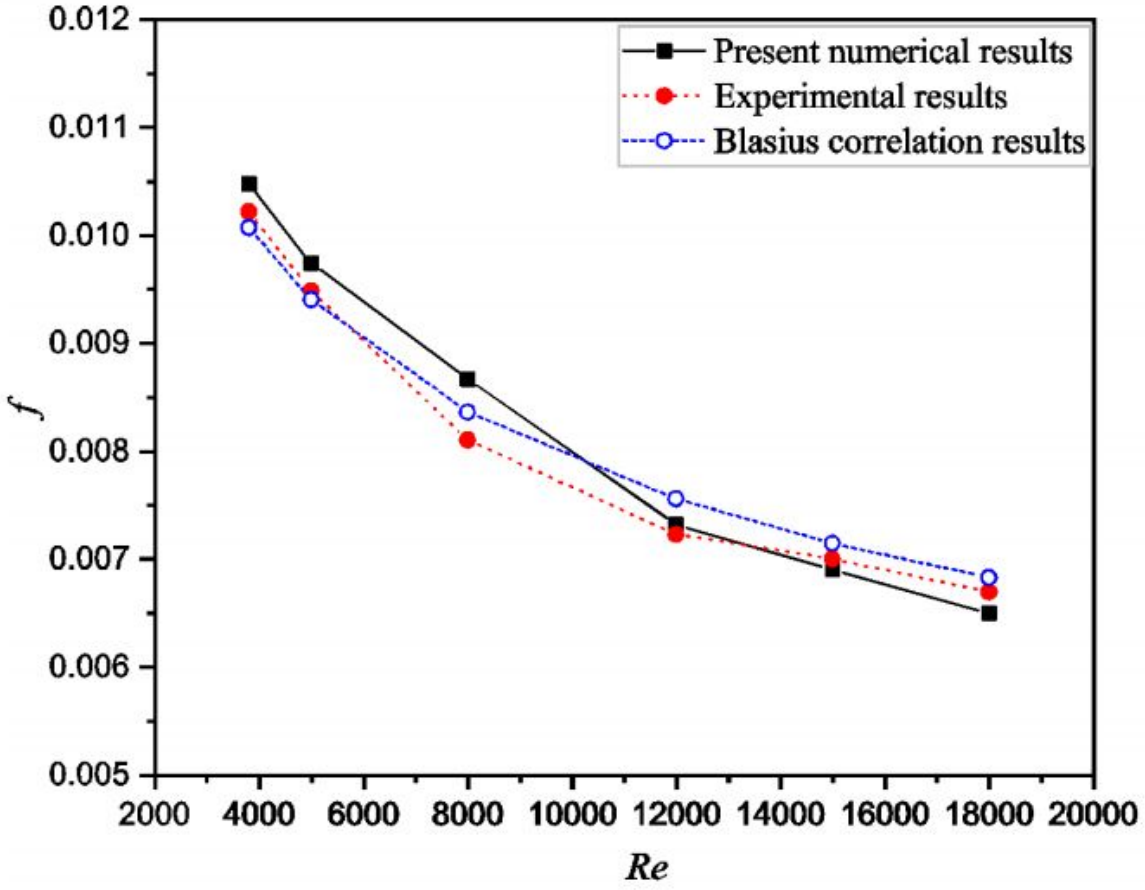

Figure 6.4: Comparison among numerical, experimental and predicted results of friction factor for smooth duct.

number (14000 and 19000). The highest values of h_x are seen at duct inlet where the thickness of the boundary layer is minimum and diminishes gradually to fully developed values. Moreover, largest and smallest values of h_x are found in triangular and semi-ellipse cross-sectional SAHs. This is because, among all cross-sectional SAH and for same Reynolds number, the highest and lowest magnitude of velocity are observed at the inlet of triangular and semi-ellipse cross-sectional duct, respectively, as their corresponding characteristic diameter are different. In addition, it is evident from the Fig. 6.6 that with the rise of Re, the values of h_x are also increasing in all cross-sectional SAHs due to enhanced turbulent intensity inside the duct of SAHs (see in Fig.6.7).

In order to show the effect of cross-section on the thermal performance, the variation of turbulent intensity (TI) at the center of SAHs along the axial length is depicted in Fig.7. The values of TI decrease with an increase of the length of the duct due to increased hindrance along the fluid flow. It is clear from Fig.6.7 that the descending order of TI in different cross-sectional SAHs are triangular > rectangular > trapezoidal > semi-ellipse. Higher values of turbulent intensity mean a more significant mixing between cold and hot fluid. Consequently, the local heat

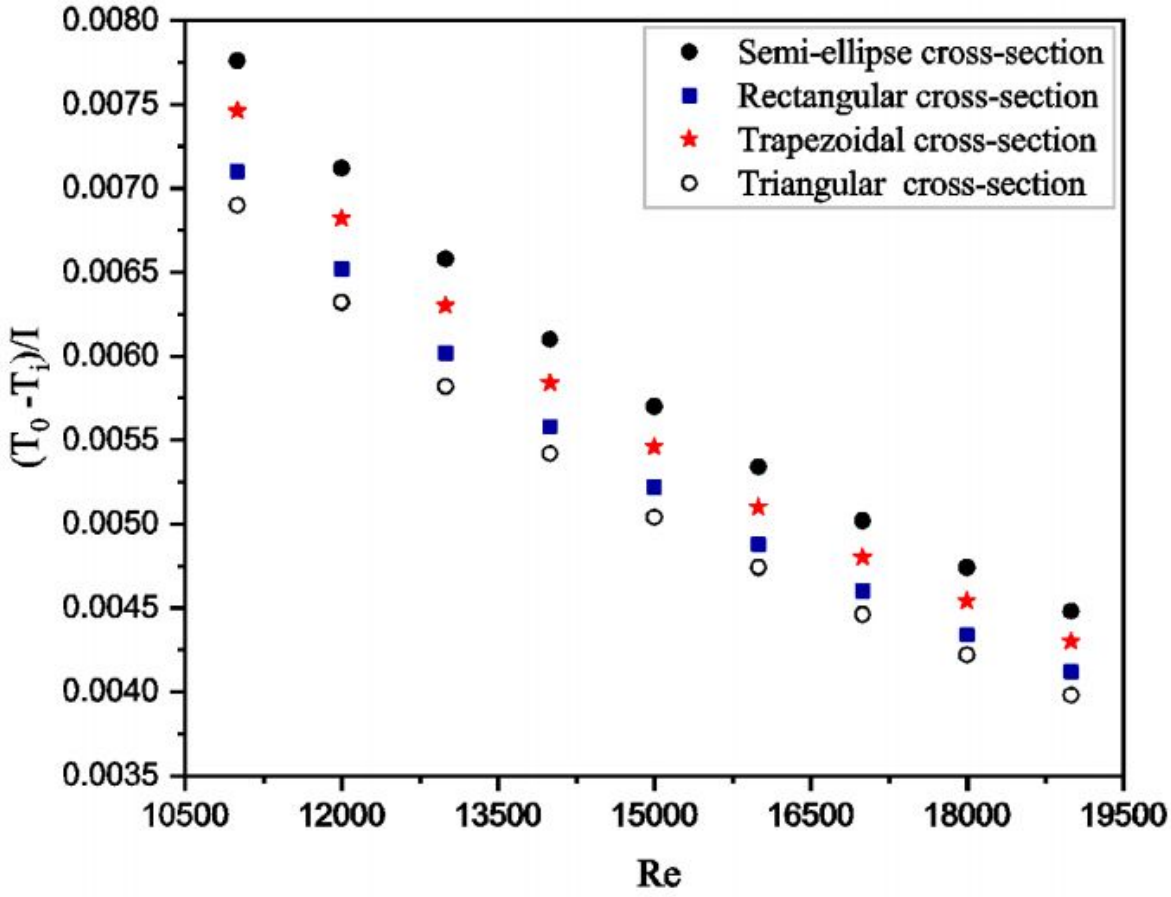

Figure 6.5: Variation of temperature factor, $\left(\frac{T_0-T_i}{I}\right)$ of various cross-sections of SAH duct for the range of Re 11000 – 19000.

transfer coefficients are found in descending order as triangular > rectangular > trapezoidal > semi-ellipse (see in Fig.6.6).

The term thermal effectiveness, $\varepsilon = \left(\frac{T_0-T_i}{T_{pm}-T_i}\right)$ is a measure of thermal characteristics associated with SAH device. The higher effectiveness value represents the higher thermal performance of SAH. Fig. 6.8 shows the variation in thermal effectiveness with temperature factor, $\left(\frac{T_0-T_i}{I}\right)$ of various cross-sections of SAH duct for the range of Reynolds number 11000 – 19000. The thermal effectiveness values of SAH increases with increasing the value of temperature factor. With an increase of Re, the heat transfer coefficient between the absorber surface and working fluid is enhanced due to an increase in turbulence intensity inside the duct, leading to reduced thermal boundary layer thickness. Therefore, absorber surface temperature of SAH decline, and consequently outlet temperature of air increase. Enhancement in heat transfer coefficient signifies the improvement in the rate of heat transfer occurring from the absorber plate to the flowing fluid. However, the heat transfer rate improvement in the semi-ellipse cross-section design is more compared to other cross-section design (see Fig.6.9). The maximum percentage enhancement in thermal effectiveness for SAH duct having semi-ellipse, rectangular and trapezoidal

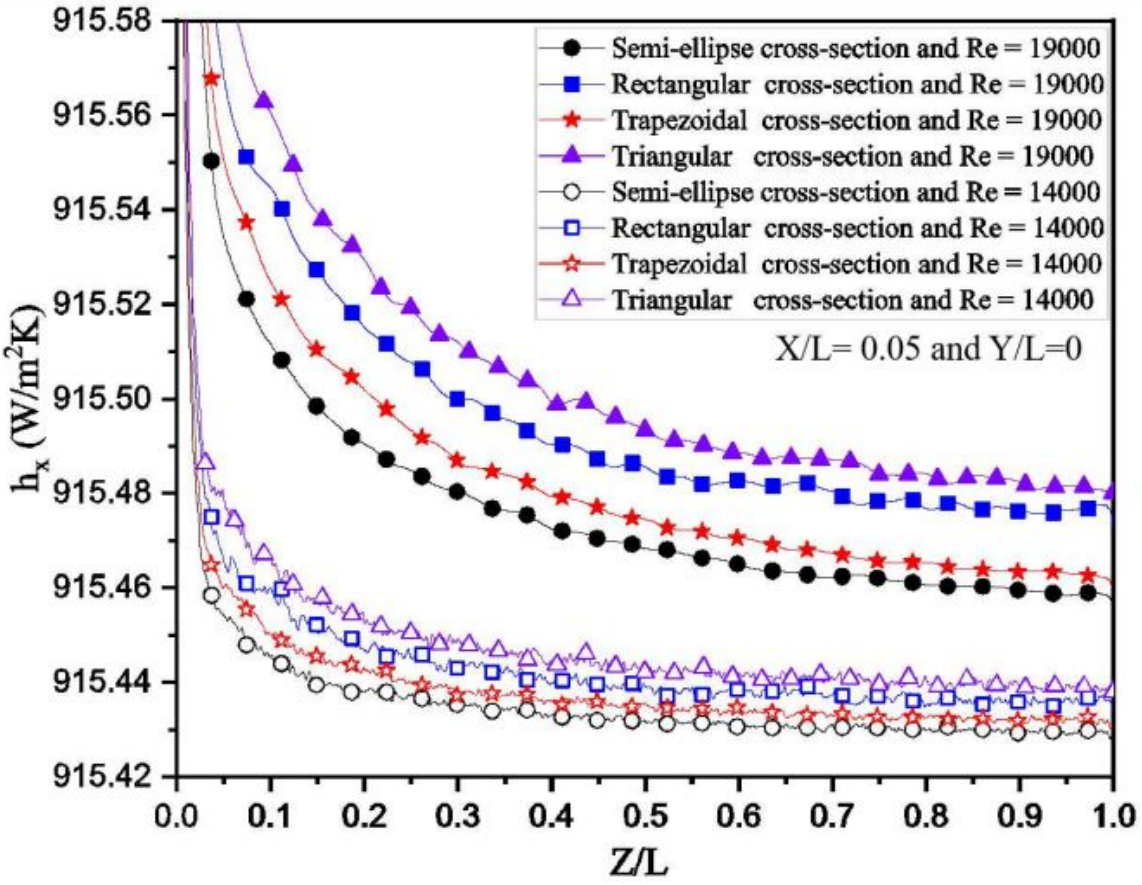

Figure 6.6: Variation of local heat transfer coefficient along the length of absorber plate of different cross-sectional SAHs for given values of Re.

cross-section are approximate 17%, 15% and 8%, respectively more as compared to the isosceles triangular cross-section.

Figure6.9 displays the variation of Nu with Re. The values of Nu have been found maximum for semi-ellipse and rectangular cross-sections shape of SAH duct. Higher values of Nu depict a higher heat transfer rate associated with the airflow. The turbulence generation in the air flow also plays a very crucial role in the augmentation of the heat transfer rate. Besides, the cross-section of the duct also plays a significant role, as the flow behaviour varies according to the duct's cross-sectional shape. The values of local heat transfer coefficient have been found in descending order as triangular > rectangular > trapezoidal > semi-ellipse cross-sectional shapes of SAH, however, the average values of Nu have been observed maximum in semi-ellipse shape as compared to other shape. This is due to semi-ellipse cross-section duct has larger value of characteristic diameter for same cross-sectional area condition. The percentage enhancement ranges in the values of Nu in SAH duct having for semi-ellipse, rectangular and trapezoidal cross-section are approximate 18 – 13%, 15 – 12% and 9 – 6%, respectively more as compared to isosceles triangular cross-section.

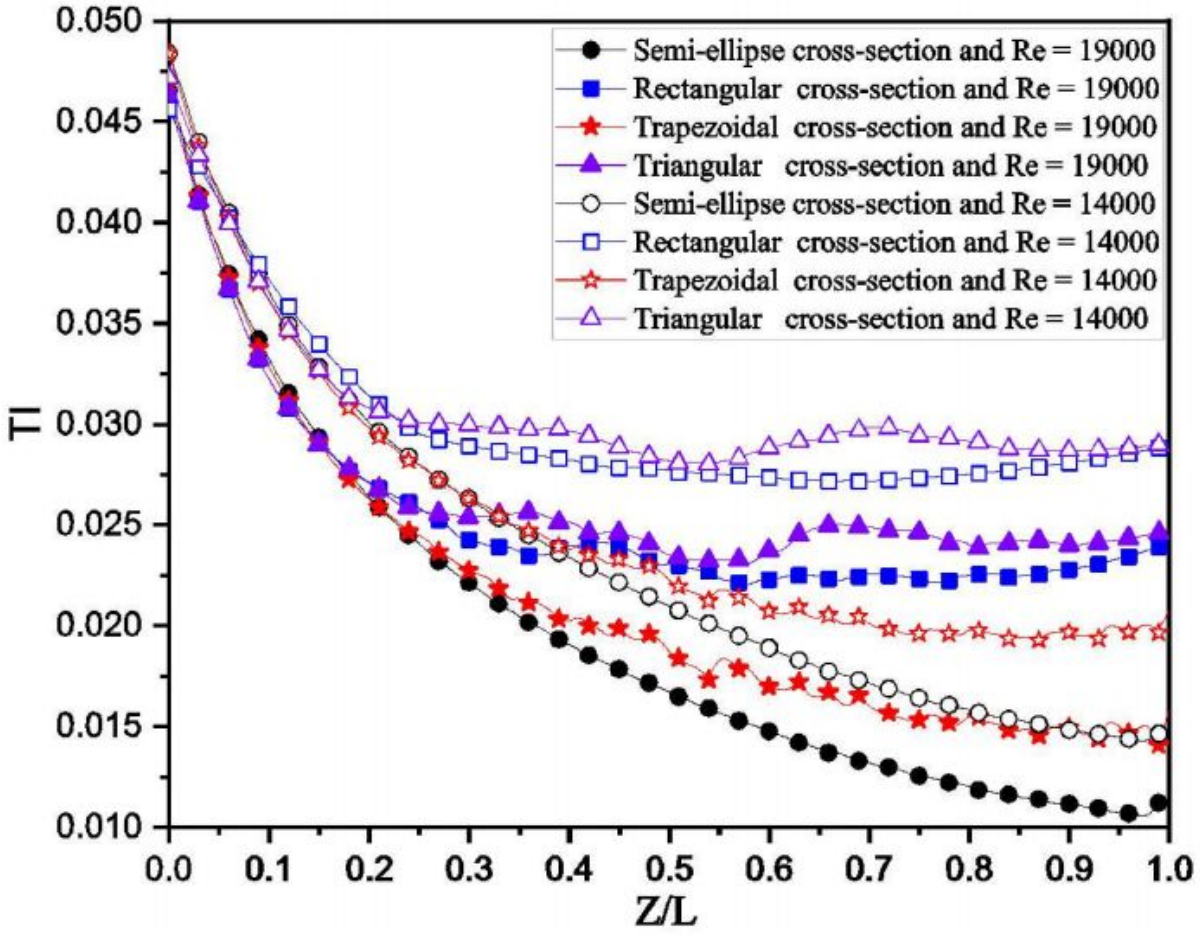

Figure 6.7: Central turbulent intensity distribution along the length of SAH with different cross-section for given values Reynolds number.

Figure6.10 illustrate the variation of wall y+ values along the length of absorber plate (Y/L = 0.0, X/L = 0.05 and Z/L) of SAHs with different cross-section for given values of Reynolds number (14000 and 19000). It is observed that wall y+ values are less than one along the whole length of the absorber plate of SAHs, which accurately capture the viscous sub-layer and transition boundary layer. Moreover, the ascending order of wall y+ values in different cross-sections of SAHs are semi-ellipse < trapezoidal < rectangular < triangular. Higher value of wall y+ means more values of wall shear stress. Consequently, more pressure drops occur across the duct of SAHs (see in Fig.6.11). It is also found that with the rise of Reynolds number, the values of wall y+ increase.

Figure6.11 shows the variation of ΔP for the range of Re 11000-19000 for different cross-sections of SAH duct. The ΔP indirectly represents the hydraulic performance of SAH. Higher the values of ΔP, the greater would be the hydraulic losses. Consequently, more pumping power requirement would enhance the operating cost of SAHs. From Fig.6.11, it is clear that ΔP increases with a rise of Re. The maximum percentage increase of ΔP for SAHs having the isosceles

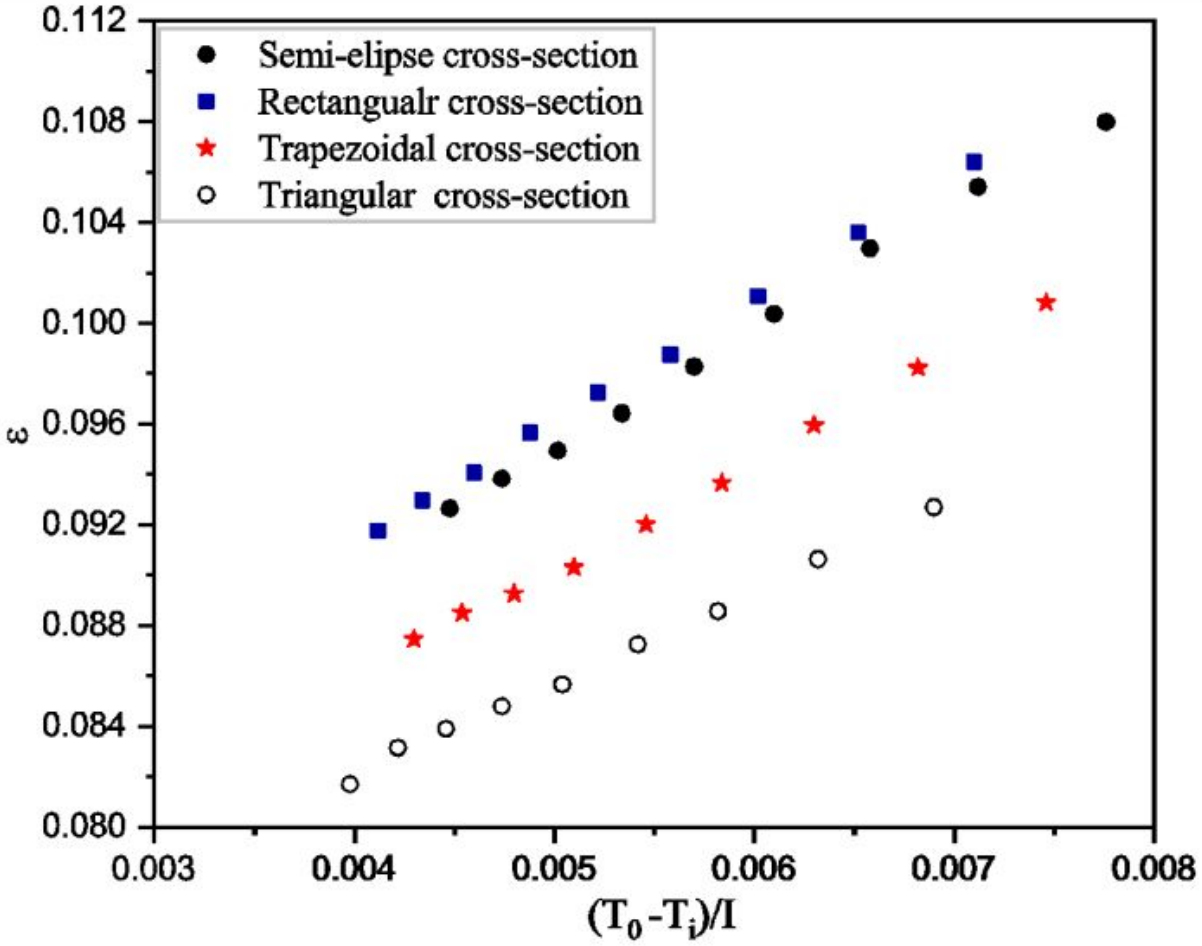

Figure 6.8: Variation in effectiveness (ε) with respect to temperature factor, $\left(\frac{T_0-T_i}{I}\right)$ for various cross-sections of SAH duct for the range of Re 11000 – 19000.

triangular, rectangular and trapezoidal are approximately 40%, 30% and 8%, respectively more as compared to semi-ellipse cross-section. Thus, it is established that SAH with ellipse cross-section would have lower operating cost as compared to other cross-sectional shapes of SAHs.

6.4.2 *Results of the best cross-section shape with corrugated SAH*

In the previous section, it was observed that semi-elliptical cross-section shows comparatively higher thermal performance than other cross-section designs investigated. In SAH designs, cross section alone is not sufficient to enhance the performance significantly. In this section, we present further design avenues to improve the thermal performance. The wavelength of waviness and amplitude are optimized for higher thermal performance.

The heat transfers rate from the wavy absorber plate to working fluid for the constant heat flux in the best cross-section shape (semi-ellipse) SAH is depicted in the form of Nusselt num-

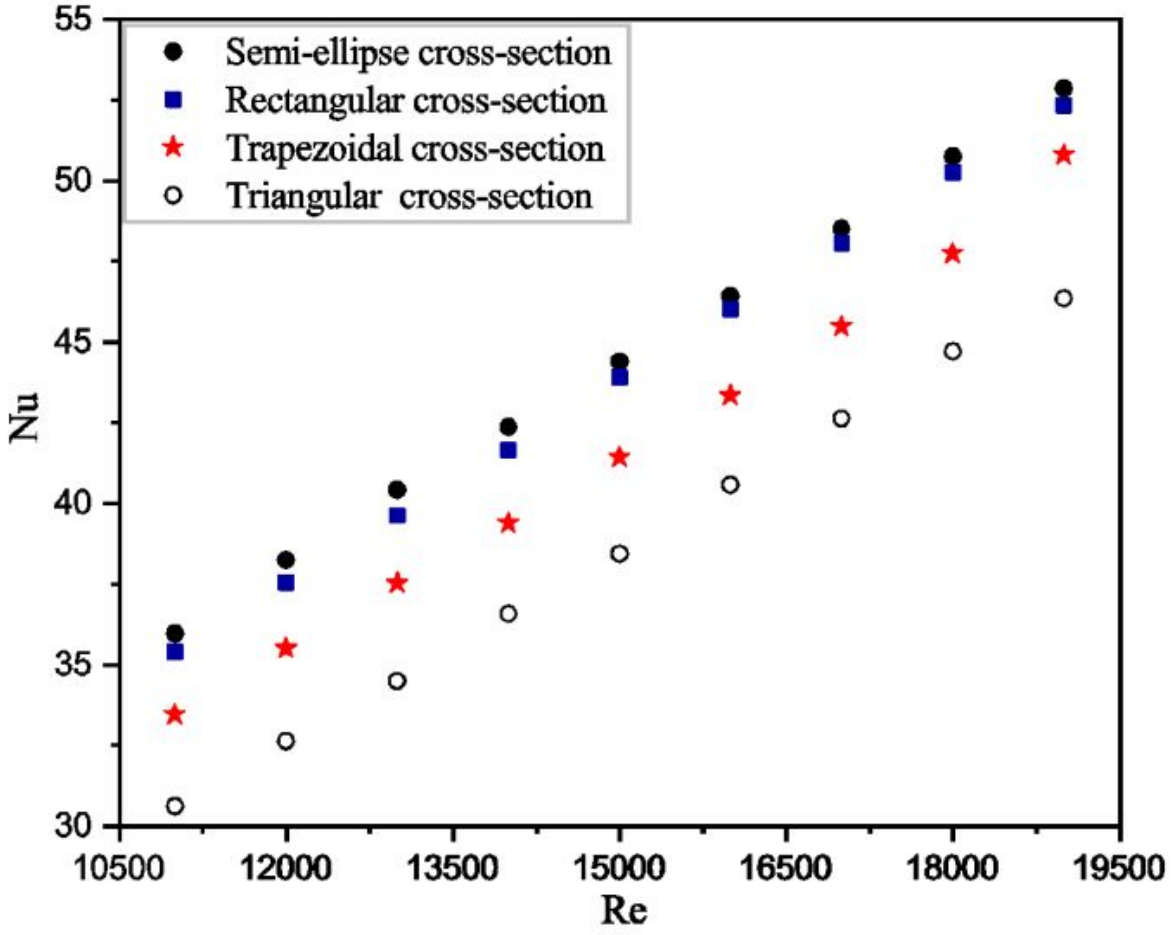

Figure 6.9: Variation of Nu with respect to Re in the range of 11000 – 19000, at the fixed value heat flux of 500 W/m^2.

ber (Nu) and Nusselt number enhancement ratio (Nu/Nu_s) in Fig.6.12 and 6.13 respectively. The Nu/Nu_s is the ratio of the Nu for SAH with wavy absorber surface to the Nu for smooth absorber surface of SAH [35]. It is seen from Fig.6.12 that Nu increase with an increase of Re for all relative roughness amplitudes (A/D_h) and relative roughness wavelengths (λ/D_h). This is due to increase in turbulent intensity inside the duct, enhancing the mixing of cold and hot fluid and reducing the thermal boundary layer thickness. Subsequently, rate of heat transfers from wavy absorber to working fluid increases. It is noticed that Nu increases with the rise of relative roughness amplitude (A/D_h) and achieve maximum value at $A/D_h = 0.12$ for all λ/D_h. The Nu values acquired by the $A/D_h = 0.04$,0.08 and 0.12 at $\lambda/D_h = 0.8$ are respectively in the range of38 – 45%, 149 – 181% and 211 – 220% larger than that of smooth semi-ellipse cross-section. It is also observed that Nu decline with increase of the λ/D_h and at $\lambda/D_h = 0.8$ yield maximum value of Nu. This is because that smallest λ/D_h creates more number of impingement point and produces more turbulence near the hot absorber, which rupture the boundary layer and consequently increase the rate of heat transfer. It can also be seen from Fig.6.13 that

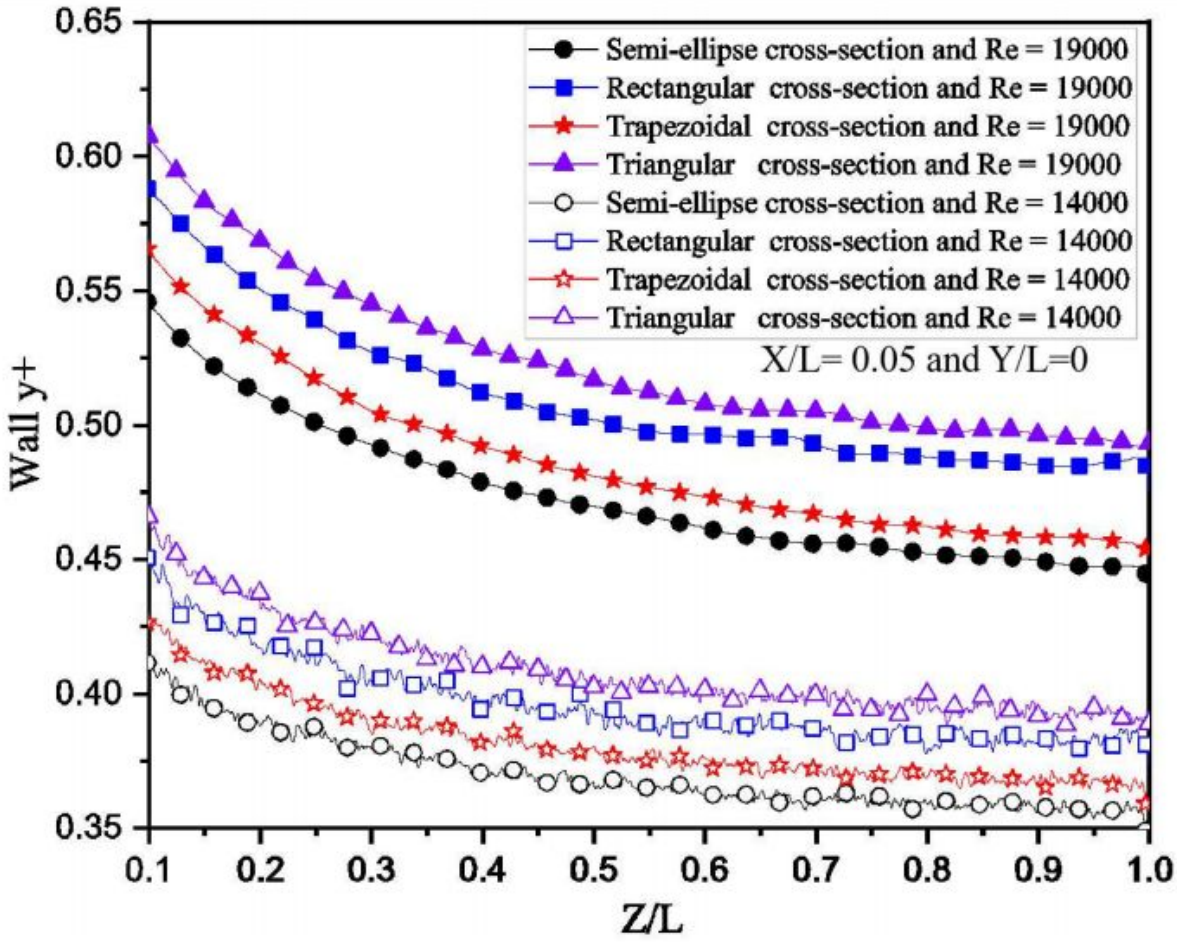

Figure 6.10: Wall y+ distribution along the length of absorber plate for different cross-sectional solar air heater at given values of Reynolds number

Nu enhancement ratio decline with increase of Re for all combination of A/D_h and λ/D_h. The maximum value of the Nu enhancement ratio has been observed at optimum wavy roughness parameters, i.e., relative roughness amplitude and relative roughness wavelength of 0.12 and 0.8, respectively, for the range of Re 11000 – 19000.

The effect of wavy geometrical parameters i.e., relative roughness amplitude (A/D_h) and relative roughness wavelength (λ/D_h) on thermal effectiveness of corrugated SAH with semi-ellipse cross-section for given values of Re are depicted in Fig.6.14. It is clear that both thermal effectiveness and temperature factor increase with increase in A/D_h and decline in λ/D_h respectively. Since increase in A/D_h and diminish in λ/D_h facilitates increase in flow passage area and generates strong vortex flow near the wavy wall boundaries, it produces more direct impingement zones. Due to improved heat transfer rate, the temperature of the absorber plate decreases and outlet air temperature increases. This phenomenon can also be seen from the contour of temperature, as shown in Fig.6.15. Designs with $\lambda/D_h = 1.6$ and 0.8 show maximum and minimum temperature respectively. A close view of Fig.6.14 discloses that for $A/D_h = 0.12$

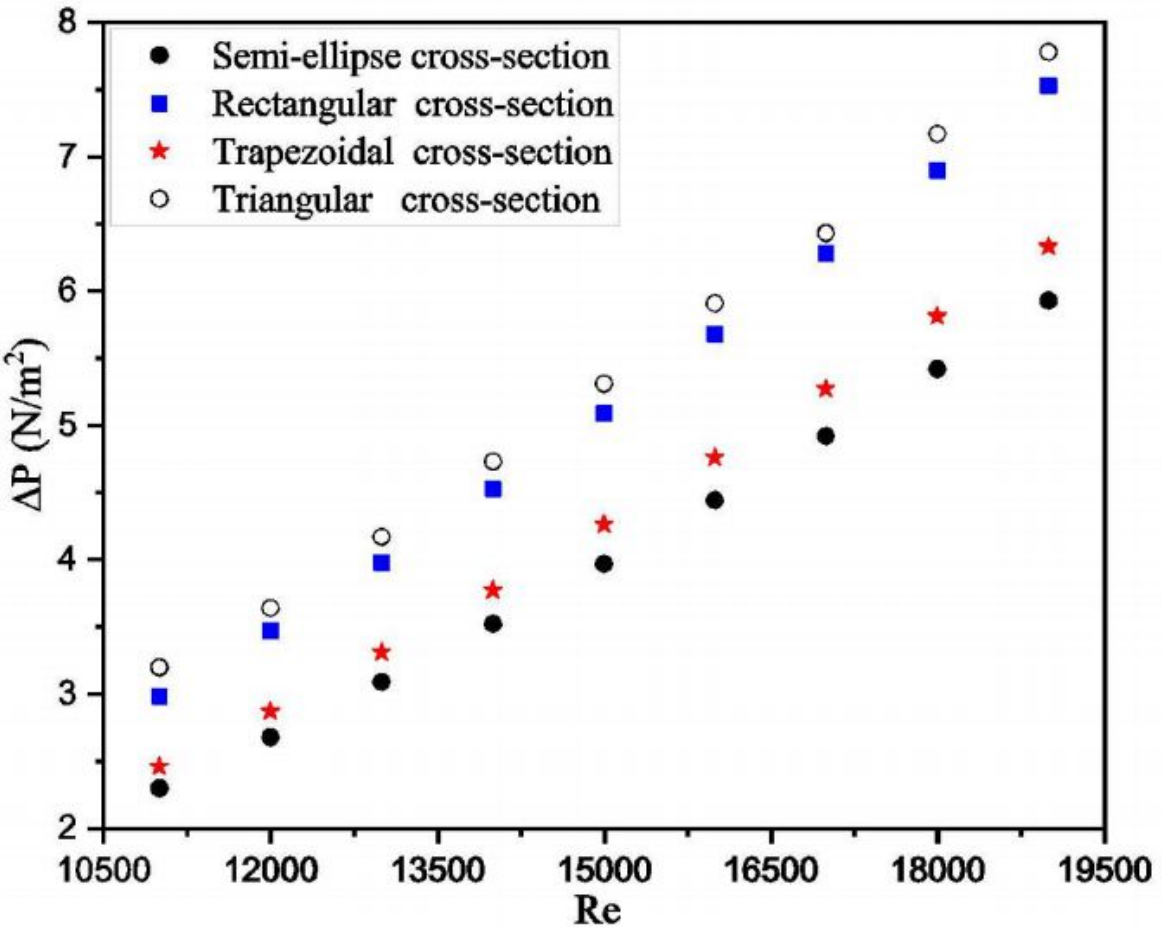

Figure 6.11: Variation of ΔP for the range of Re 11000-19000 for different cross-sections of SAH duct.

augmentation in thermal effectiveness is about 180 – 189%, 160 – 172% and 124 – 135% for $\lambda/D_h = 0.8$, 1.2 and 1.6 respectively, over smooth semi-ellipse cross-section of SAH.

Figure. 6.16 illustrate the contour plots of turbulent kinetic energy (TKE) for corrugated SAH with semi-ellipse cross-section for distinct values of relative roughness amplitude (A/D_h) and constant values of relative roughness wavelength (λ/D_h) and Reynolds number. It can be seen that strength of turbulent kinetic energy regime increases near the wavy absorber surface with increase of relative roughness amplitude. Maximum TKE is observed at $A/D_h = 0.12$. The strength of turbulence in the flow filed is proportional to turbulent kinetic energy. This can also be observed from Fig.6.12 as Nu increase with increase in A/D_h.

To demonstrate the influence of wavy roughness parameters on the flow filed, the contour plots of velocity magnitude are presented in Fig 6.17 at a fixed value of $Re = 11000$. It is observed that maximum magnitude of velocity is shifted towards the centre of duct due to wavy absorber and breaking of boundary layer near the troughs due to direct impingement. Moreover, the magnitude of velocity increases toward the centre of duct as well as near the trough of wavy

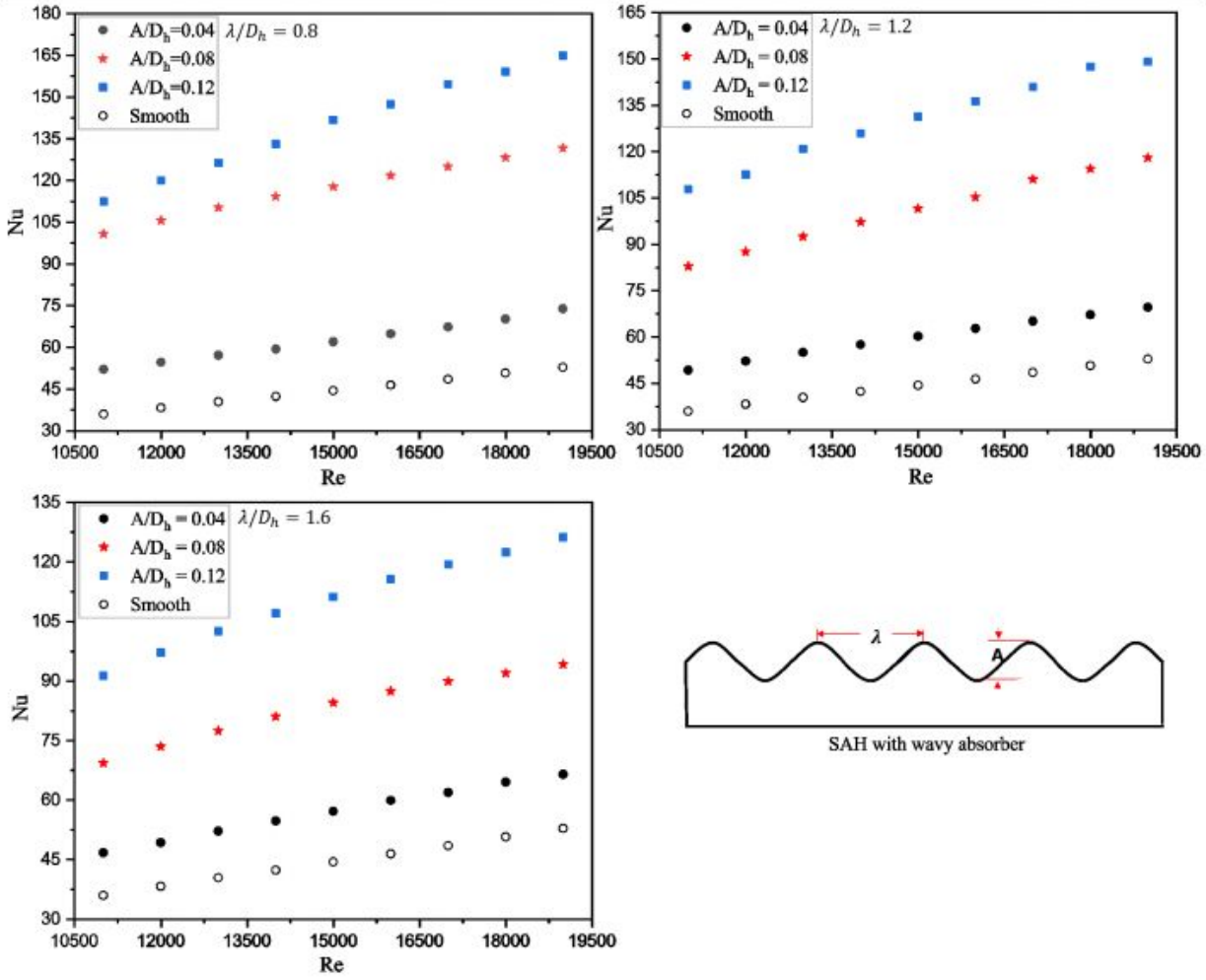

Figure 6.12: Variation of Nu vs Re for different values of A/D_h and λ/D_h

surface with increase of relative roughness amplitude. This is because a wavy surface creates obstacle in flow due to increased amplitude and produces more TKE inside the duct (as shown in Fig.6.16).

The influence of Re on the friction factor (f) and friction factor enhancement ratio(f/f_s) for corrugated SAH with semi-ellipse cross-section is presented in Fig 6.18 and 6.19, respectively. Thef/f_s is the ratio of friction factor for duct with wavy absorber plate to the friction factor for smooth duct [18]. As anticipated, f decline with increase of Re for all combination of A/D_h and λ/D_h. This decrease is due to reduction in recirculation zones near upstream and downstream of the trough and diminished boundary layer thickness with increase in Re. Therefore, the pressure gradient effect around the wavy absorber surface is lowered with the increase of Re and hence friction factor also reduces. From Fig. 6.18 it is clear that friction factor increase with increase of A/D_h for all λ/D_h and decrease with increase in λ/D_h for all A/D_h. The major losses are due to the higher flow obstruction and the large contact area with higher A/D_h and the lower λ/D_h. For the constant duct length, a small λ/D_h means large wave cycle in the duct

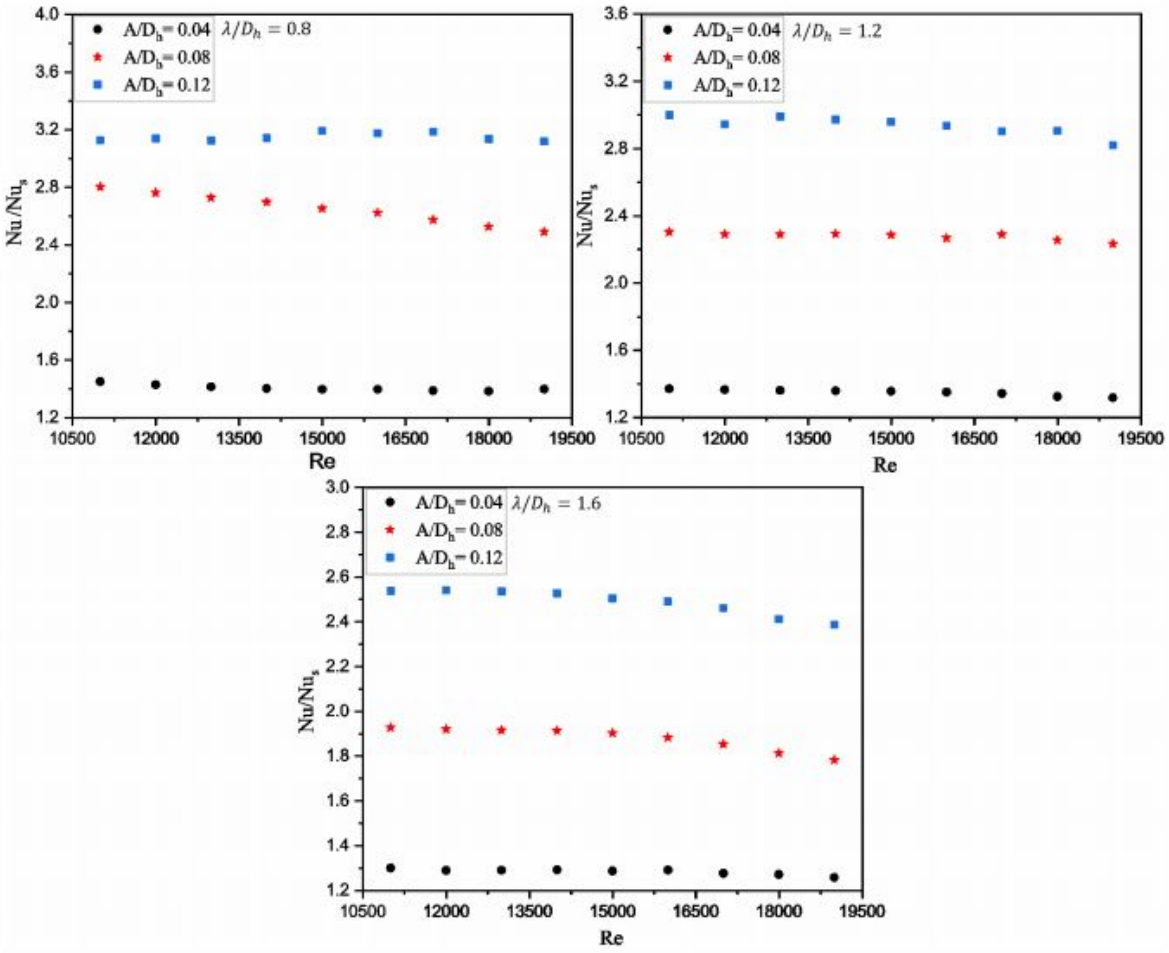

Figure 6.13: Variation Nu/Nu_s vs Re offor different values of A/D_h and λ/D_h

and hence, higher flow blockage. The friction factor values for $\lambda/D_h = 0.8$ at fixed $A/D_h = 0.12$ are approximately $18-22\%$ and $74-81\%$ higher than those $\lambda/D_h = 1.2$ and $\lambda/D_h = 1.6$ respectively. Fig. 6.19 shows that using a wavy absorber leads to a significant rise in f compared to a smooth absorber by 1.25 to 3.19 times. For $\lambda/D_h = 0.8$, the increase in f over smooth duct are about $1.38-1.44$, $2.49-2.80$, and $3.11-3.19$ times for $A/D_h = 0.04$, $A/D_h = 0.08$ and $A/D_h = 0.12$ respectively. It is also noticed that an increase in λ/D_h corresponds decline in both Nu and f, thus diminishing λ/D_h may not be an effective technique to decrease the pressure drop across the corrugated SAH with semi-ellipse cross-section.

Figure 6.20 indicates that Nu/f variation with Re for different values of relative roughness amplitude (A/D_h) and relative roughness wavelength (λ/D_h). The Nu/f indirectly represents thermo-hydraulic characteristic of SAH, higher the value, greater would be the heat capturing capability of the flowing air with minimum possible friction losses. The values of Nu/f increases with increase of Re for constant value of wavy roughness parameters. This increase is due to decrease of friction factor across the duct. It is worth noticing that Nu/f decrease with rise in A/D_h.The maximum and minimum values of Nu/f is observed at $A/D_h = 0.04$ and A/D_h= 0.12

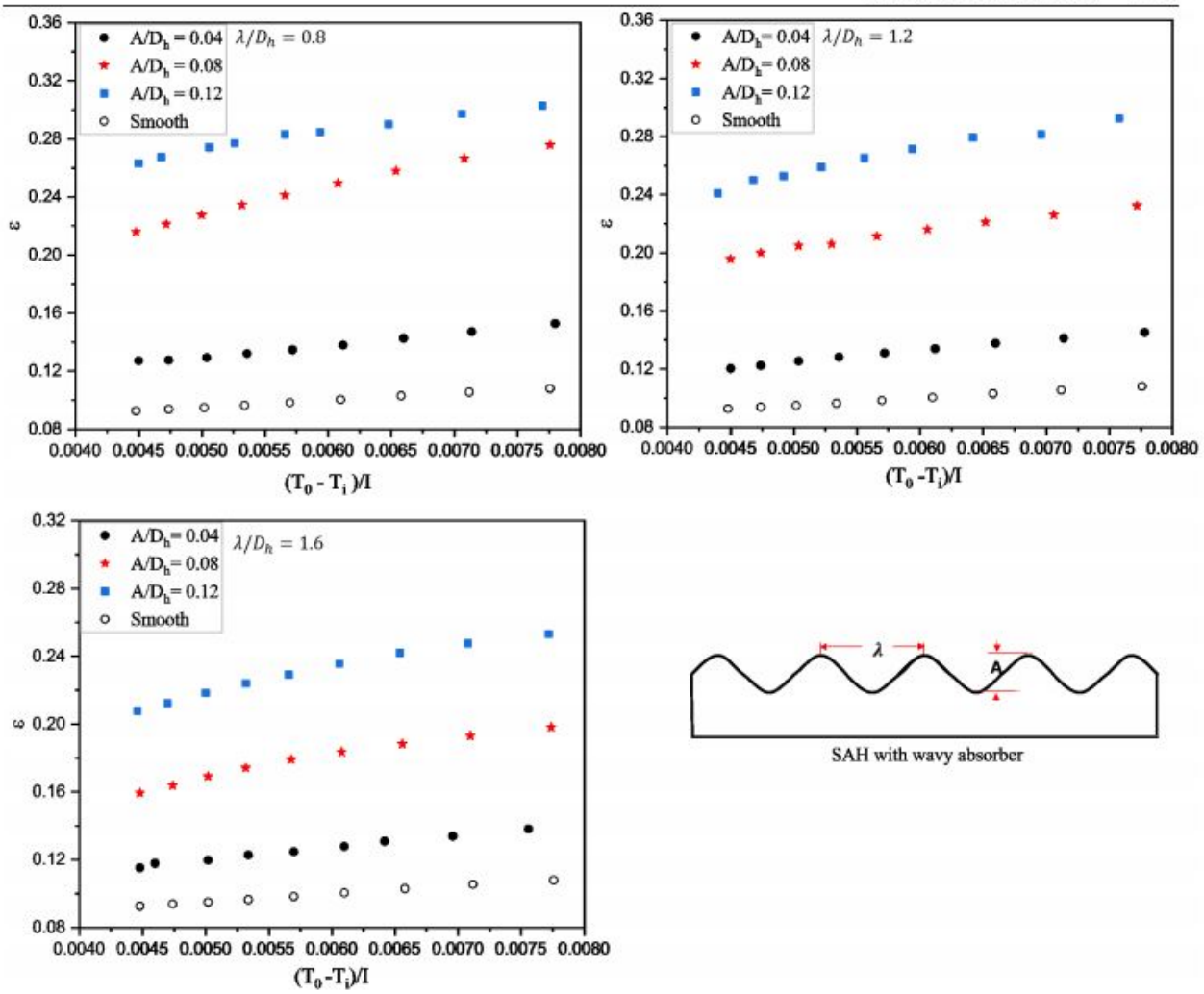

Figure 6.14: Variation of thermal effectiveness with temperature factor for different values of A/D_h and fixed value of λ/D_h for a range of Re 11000 – 19000.

respectively for all λ/D_h in the range of Re 11000-19000.

To understand the hydraulic performance of corrugated SAH having semi-ellipse cross-section, Fig.6.21 depicts the contour plot of static pressure for distinct values of A/D_h. The increase in A/D_h, increase the disturbance of flow structure at crest and troughs due to sudden expansion and contraction of cross-sectional area of flow passes throughout the whole length of duct. This interruption of flow causes additional momentum loss which lead to develop high static pressure drop. The maximum static pressure drop occur at $A/D_h = 0.12$. The static pressure drop at $A/D_h = 0.12$ is approximately 4 and 2.5 times more as compared to $A/D_h = 0.04$ and 0.08 respectively. The higher static pressure drop causes higher frictional losses, consequently more pumping power required but higher heat transfer comes at the cost of higher losses. Therefore, optimise wavy roughness parameters ($A/D_h = 0.04$ and $\lambda/D_h = 0.8$) is a preferred design. This can be noticed from the overall thermohydraulic performance ($Nu/\Delta P$) shown in Fig 6.20.

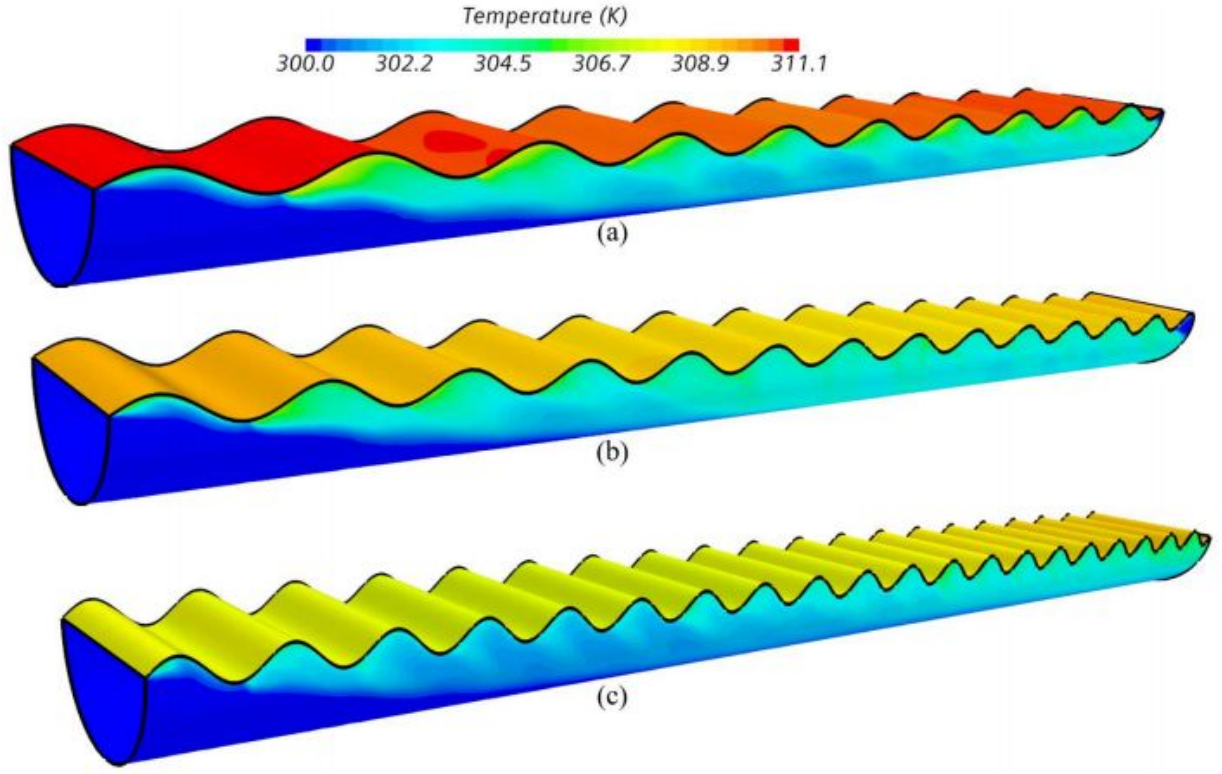

Figure 6.15: Contour plots of temperature at $Re = 19000$ and $A/D_h = 0.12$ for (a) $\lambda/D_h = 1.6$, (b) $\lambda/D_h = 1.2$ and (c) $\lambda/D_h = 0.8$.

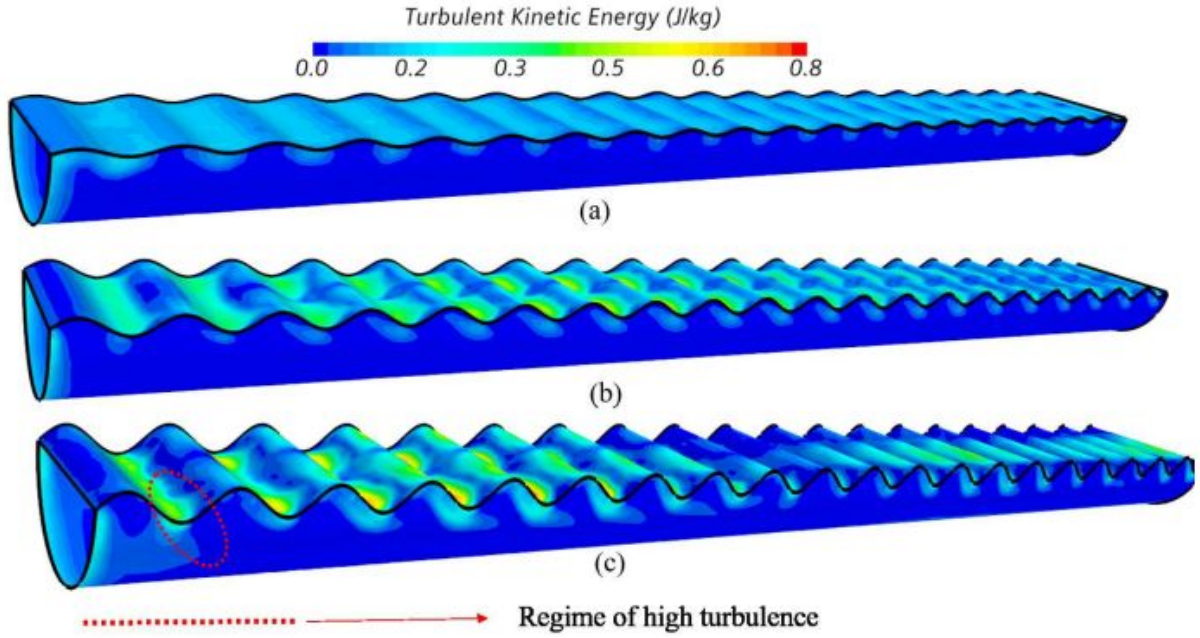

Figure 6.16: The contour of TKE at $Re = 11000$ and $\lambda/D_h = 0.8$ for (a) $A/D_h = 0.04$ (b) $A/D_h = 0.08$ and (c) $A/D_h = 0.12$.

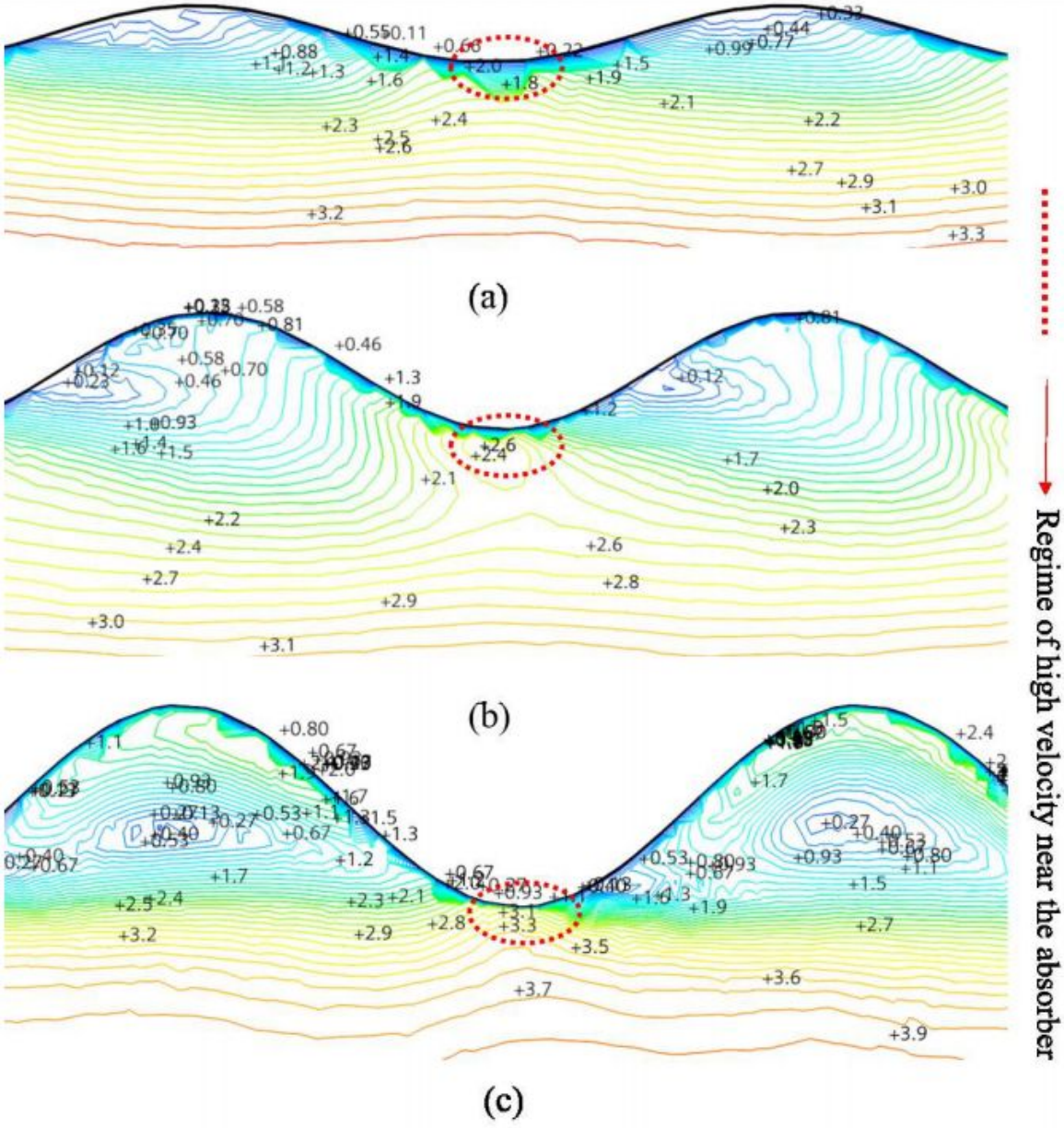

Figure 6.17: The contour plots of velocity magnitude at Re = 11000 and λ/D_h = 0.8 for (a) $A/D_h = 0.04$ (b) $A/D_h = 0.08$ and (c) $A/D_h = 0.12$.

Figure.6.22 illustrates the local wall shear stress variation with respect to duct length of corrugated SAH with semi-ellipse cross-section for different values of A/D_h. It can be seen that significant fluctuations of higher magnitude in shear stress is observed for higher $A/D_h = 0.12$ even in the downstream troughs, suggesting significant fluctuations in flow field and turbulence generation. However, for $A/D_h = 0.08$, fluctuations in shear stresses are of nearly uniform magnitudes, suggesting uniform heat transfer across the duct length near the troughs. For further low A/D_h ratio, shear stress magnitude is small and thus offers low heat transfer from heated plates to the flowing air. It is to be noted that, higher heat transfer comes at the cost of higher

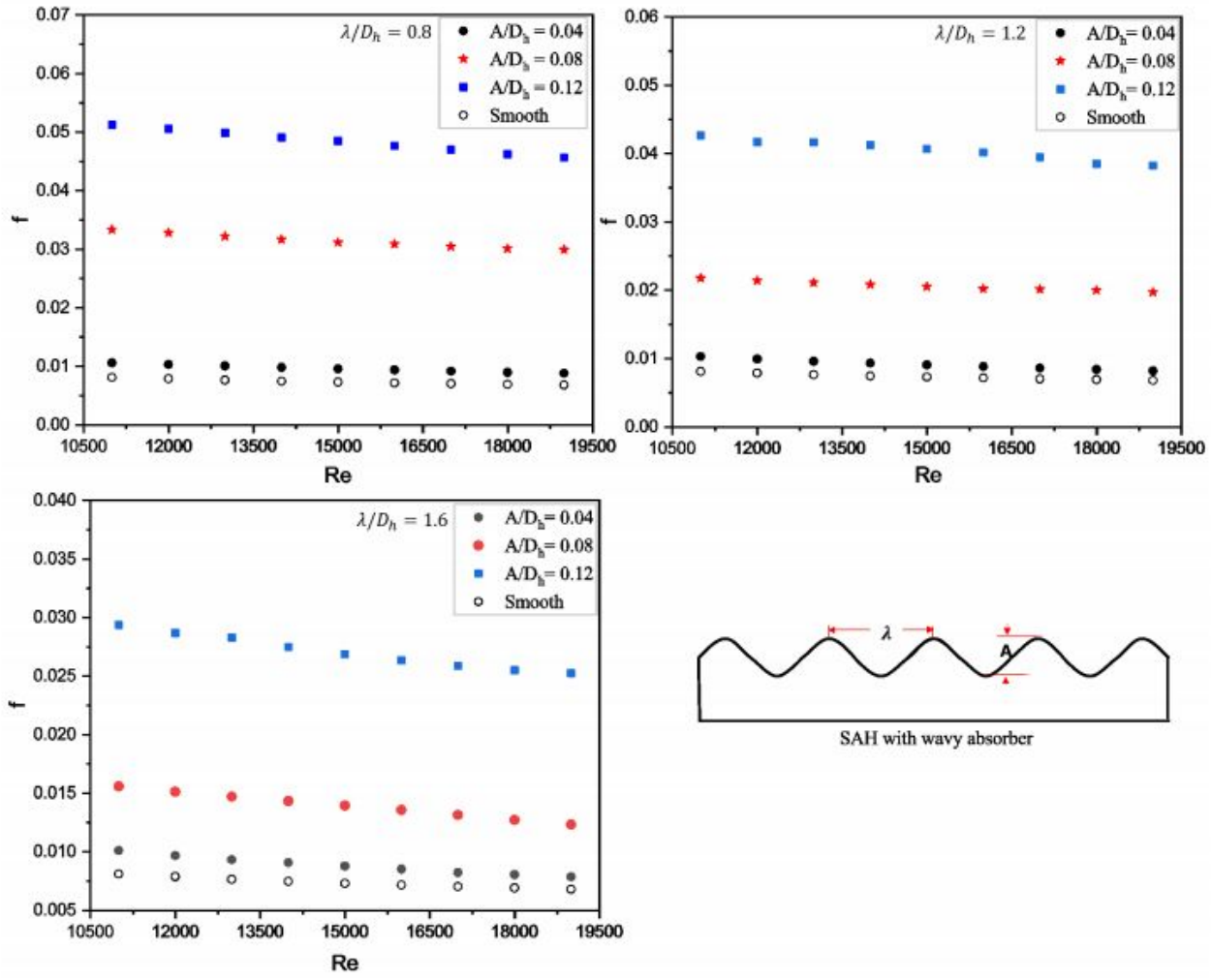

Figure 6.18: Plots of f with Re for distinct values of A/D_h and λ/D_h in corrugated SAH with semi-ellipse cross-section.

losses which may finally increase the cost of pumping power. Observation in shear stress variation described above corroborates the findings in the local velocity variations (see Fig.6.17).

6.4.3 *Empirical correlation development for Nu and f*

Multi-variable regression analysis method is used to develop the empirical correlation for SAH with semi-ellipse cross-section integrated with wavy absorber by relating CFD data of Nu and f in term of Re, A/D_h and λ/D_h. The estimated relationships for Nu and f are display in Eqs.6.25 and 6.26 respectively. The predicted data from developed relationships are compared with CFD data and found the absolute average percentage deviation of 3.68 and 9.84 for Nu and f respectively. Considering this reasonable variation, these relations can be used to predict the thermo-hydraulic performances for various geometrical parameters.

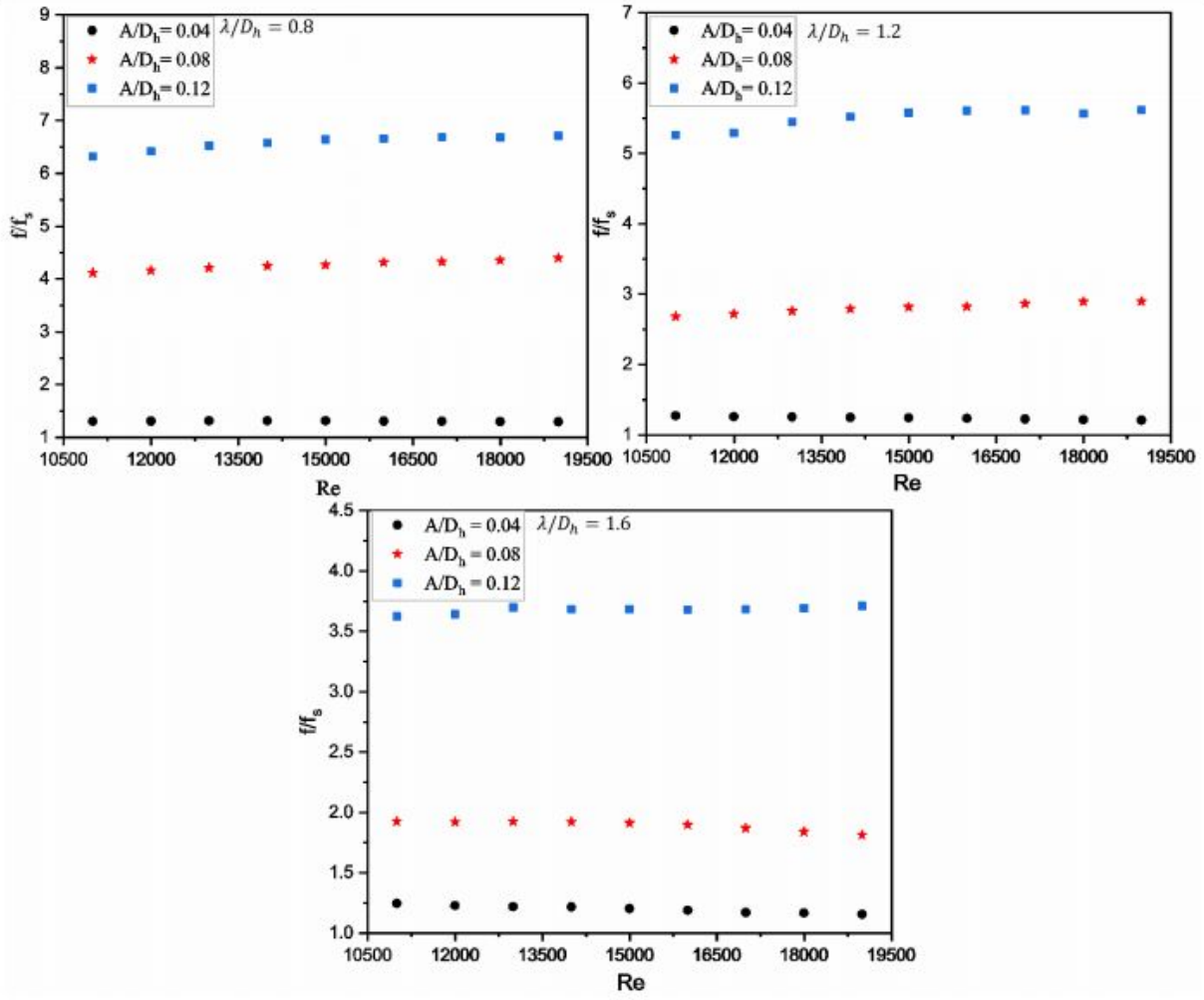

Figure 6.19: Plots of f/f_s with $Re$for distinct values of A/D_h and λ/D_h in corrugated SAH with semi-ellipse cross-section.

$$Nu = 0.6Re^{0.61}\left(\frac{A}{D_h}\right)^{-0.08}\left(\frac{\lambda}{D_h}\right)^{-0.23} exp\left[-0.14\left\{ln\left(\frac{A}{D_h}\right)\right\}^2\right] exp\left[-0.37\left\{ln\left(\frac{\lambda}{D_h}\right)\right\}^2\right] \quad (6.25)$$

$$f = 66.7\,Re^{-0.31}\left(\frac{A}{D_h}\right)^{2.6}\left(\frac{\lambda}{D_h}\right)^{-0.6} exp\left[0.25\left\{ln\left(\frac{A}{D_h}\right)\right\}^2\right] exp\left[-0.64\left\{ln\left(\frac{\lambda}{D_h}\right)\right\}^2\right] \quad (6.26)$$

6.5 Conclusions

Flow interaction of the heated fluid in the flow channel of the SAH affects both its hydraulic and thermal performance. To enhance the thermal performance of this device, a systematic investigation has been performed numerically for a large range of flow and geometric parameters. In the first stage, conventional rectangular channel design performance was compared with the

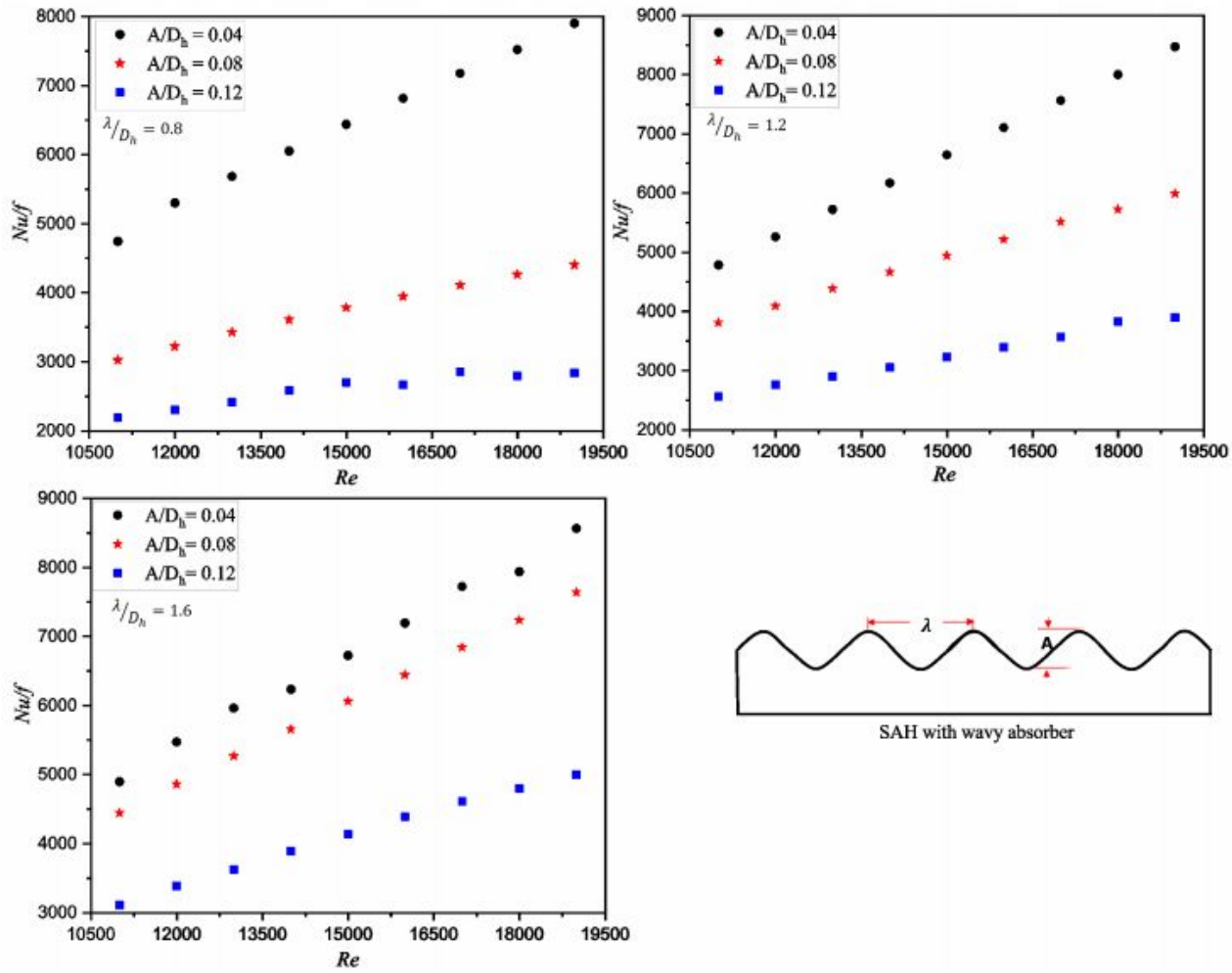

Figure 6.20: Plots of Nu/f with Re for distinct values of A/D_h and λ/D_h in corrugated SAH with semi-ellipse cross-section.

non-rectangular designs and results are discussed in terms of temperature factor$\left(\frac{T_0-T_i}{I}\right)$, thermal effectiveness($\varepsilon$), Nusselt number($Nu$), Nusselt number per unit friction factor (Nu/f) and friction factor(f). In the second stage, best configuration channel design was further investigated to enhance its performance by introducing sinusoidal wavy absorber with relative roughness wavelength (λ/D_h) and relative roughness amplitude (A/D_h). Two new correlations were proposed to predict the thermal and hydraulic characteristics of the device. Following are some of the important observations:

- The maximum percentage increase of 10% in temperature factor has been found for SAH duct having semi-ellipse cross-section compared to conventional SAH (rectangular cross-section), while the next maximum was 5% increase for the trapezoidal cross-section. For unit pressure drop or losses, semi-ellipse cross-section design is the best choice considering the compromise between thermal and hydraulic performance.

- The value of Nu/Nu_s and f/f_s have been observed maximum at wavy roughness parameters, i.e., A/D_h and λ/D_h of 0.12 and 0.8, respectively for the 11000 – 19000 range of Reynolds number.
- The value of Nu/f flattens at higher Reynolds number and decreases with increase in relative roughness amplitude.
- Two empirical correlation have been developed for Nu and f for best cross-section with sinusoidal wavy absorber SAH. The predictions from these relationships agree well with numerical data and have absolute average percentage deviation of 3.68 and 9.84 for Nu and f, respectively.

The designs and data presented in the paper would help the scientific community in developing thermally efficient designs of solar air heaters to harness the solar energy.

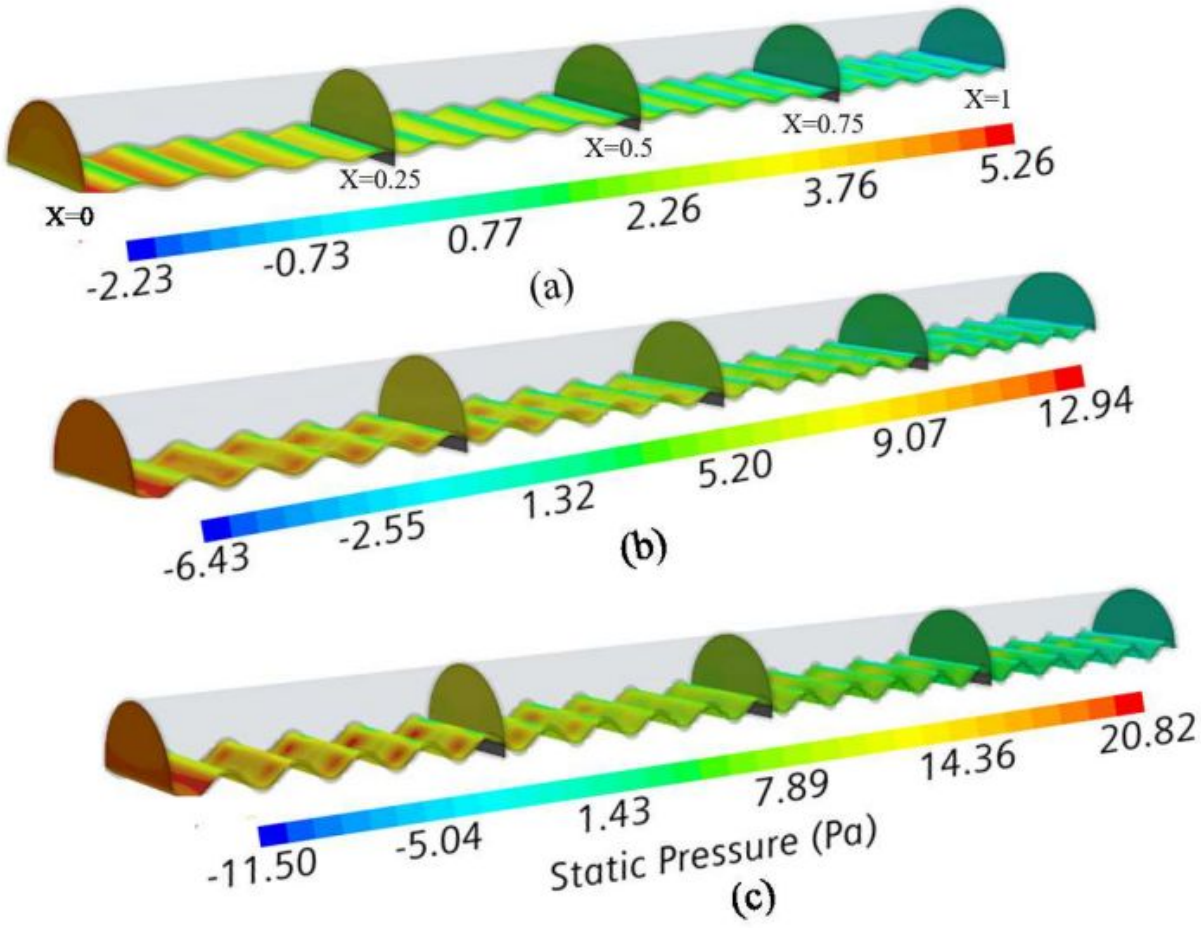

Figure 6.21: The contour plots of static pressure at $Re = 11000$ and $\lambda/D_h = 0.8$ for (a) $A/D_h = 0.04$ (b) $A/D_h = 0.08$ and (c) $A/D_h = 0.12$.

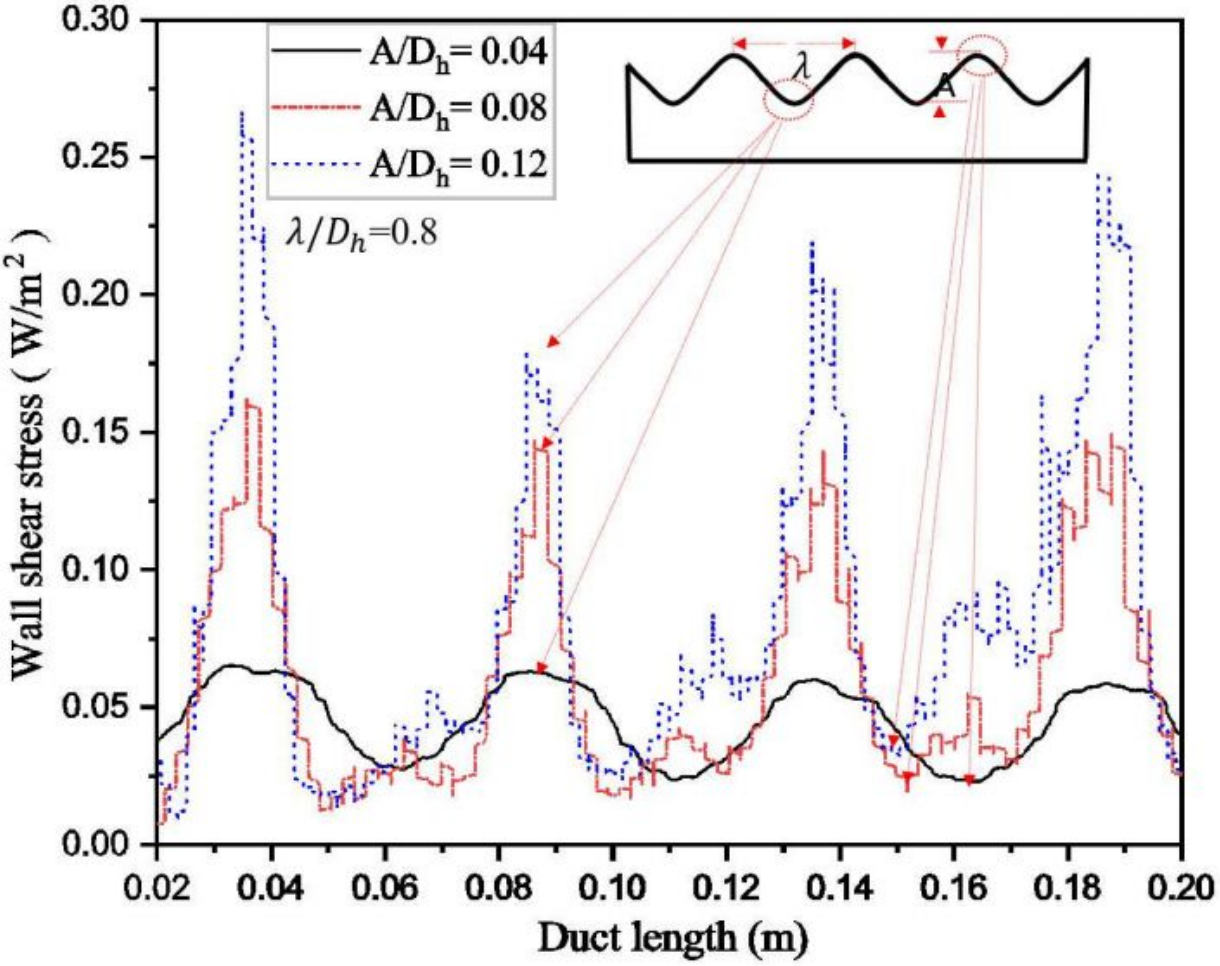

Figure 6.22: Variation of local wall shear stress along the length of duct of SAH with dissimilar values of A/D_h for fixed value of Re and λ/D_h of 11000 and 0.8 respectively.